2013

STRUCTURAL CONTROL OF A SMALL-SCALE TEST-BED SHAKER STRUCTURE USING A SPONGE-TYPE MAGNETO-RHEOLOGICAL FLUID DAMPER

Benjamin D. Winter
Michigan Technological University

STRUCTURAL CONTROL OF A SMALL-SCALE TEST-BED SHAKER STRUCTURE USING A SPONGE-TYPE MAGNETO-RHEOLOGICAL FLUID DAMPER

By

Benjamin D. Winter

A REPORT

Submitted in partial fulfillment of the requirements for the degree of

MASTER OF SCIENCE

In Civil Engineering

MICHIGAN TECHNOLOGICAL UNIVERSITY

2013

This thesis has been approved in partial fulfillment of the requirements for the Degree of MASTER OF SCIENCE in Civil Engineering.

Department of Civil and Environmental Engineering

Report Advisor:	*Dr. R. Andrew Swartz*
Committee Member:	*Dr. William Bulleit*
Committee Member:	*Dr. Qingli Dai*
Committee Member:	*Dr. Bo Chen*
Department Chair:	*Dr. David Hand*

Table of Contents

List of Figures

List of Tables

Abstract

Semi-active damping devices have been shown to be effective in mitigating unwanted vibrations in civil structures. These devices impart force indirectly through real-time alterations to structural properties. Simulating the complex behavior of these devices for laboratory-scale experiments is a major challenge. Commercial devices for seismic applications typically operate in the 2-10 kN range; this force is too high for small-scale testing applications where requirements typically range from 0-10 N. Several challenges must be overcome to produce damping forces at this level. In this study, a small-scale magneto-rheological (MR) damper utilizing a fluid absorbent metal foam matrix is developed and tested to accomplish this goal. This matrix allows magneto-rheological (MR) fluid to be extracted upon magnetic excitation in order to produce MR-fluid shear stresses and viscosity effects between an electromagnetic piston, the foam, and the damper housing. Dampers for uniaxial seismic excitation are traditionally positioned in the horizontal orientation allowing MR-fluid to gather in the lower part of the damper housing when partially filled. Thus, the absorbent matrix is placed in the bottom of the housing relieving the need to fill the entire device with MR-fluid, a practice that requires seals that add significant unwanted friction to the desired low-force device. The damper, once constructed, can be used in feedback control applications to reduce seismic vibrations and to test structural control algorithms and wireless command devices. To validate this device, a parametric study was performed utilizing force and acceleration measurements to characterize damper performance and controllability for this actuator. A discussion of the results is presented to demonstrate the attainment of the damper design objectives.

1 Introduction

The purpose of this study is to explore and test magneto-rheological (MR) damping systems for small-scale seismic test-bed apparatuses. Semi-active damping devices are of particular interest in civil engineering modeling applications because they can be used to alter damping forces in real-time through rapid changes of applied current. Small-scale semi-active dampers, like MR-dampers, can provide platforms for laboratory validation of control algorithms and communication topologies in wireless control networks. Rheological dampers have not been used in simulations due to the inherent difficulty posed by generating low force levels (*e.g.*, 0-10 N force) from such devices. Commercial devices provide a kN force range, too high for small-scale laboratory experiments. The objective of this study is to design and test a low-force MR-fluid damper suitable for small-scale lab testing. This device should behave with time-domain and frequency-domain properties that are comparable to full-scale commercial devices.

1.1 Motivation

Semi-active control testing for structural response control is currently performed in specialized large-scale testing facilities. The motivation behind this study spawns from the expense of these larger testing facilities (*e.g.*, travel expense to facilities, construction of large test-beds, and cost of commercial semi-active dampers, *etc.*). To bring this technology down to a scale that can be implemented in small-scale test-beds would allow for affordable studies to be conducted at many more sites than are presently available. Previous work in structural control has been performed by this research group at the large-scale test facility of the National Center for Research in Earthquake Engineering (NCREE) [1]. These experiments, while highly valuable, represent high stakes and costly

commitments by both the researchers, as well as the host facility in terms of time, travel cost, specimen preparation cost, energy, and labor. Testing time at facilities, such as NCREE, is a limited resource, limiting the scope and number of tests that can be performed there. Small-scale structural control test-beds can significantly enhance the experimental work that can be performed in this area. To achieve small-scale test-bed damping forces that can mimic the damping performance observed in large-scale testing with commercial devices, several challenges must be overcome. These challenges are to produce a proportional force range for comparison to large-scale damping behavior, to eliminate undesired friction to obtain as low of controllable forces as possible, to match the modal behavior of large-scale test-beds, and to match the same hysteretic damping force behavior. These challenges are discussed in depth in Section 3.

1.2 Objectives

The main objective of this study is to construct a semi-active damper that can simulate the performance of commercial-scale devices, specifically those used in the previously cited NCREE studies suitable for use in a small-scale semi-active control test-bed. Such a test-bed will serve as an affordable platform for validating the performance of structural control networks. After scaling down the forces of semi-active devices and using small-scale test-beds simulators/shakers, not only wired, but also wireless control techniques can be performed, validated, and optimized. Another objective is to capture the attributes observed in the NCREE semi-active devices in order to make direct comparisons with results obtained in those studies. The studies performed at NCREE involved a 6-story scale test structure. Each story was equipped with semi-active (magneto-rheological) dampers capable of providing forces with peak magnitudes of approximately 10% of the

individual peak story inertial forces. An important objective of this study is to match this ratio in a small-scale test-bed. This objective requires that the new damper possess very small friction forces, when turned off, yet still be capable of producing useful levels of damping forces over a workable range of input current levels. In addition, the small-scale dampers should also possess hysteretic behavior similar to the commercial devices used previously. Once these objectives are met, the resulting damper will be suitable for use in the desired small-scale laboratory test-bed.

1.3 Hypotheses

It is hypothesized that a metal foam magneto-rheological (MR) fluid device can be made to mimic the behavior of large-scale MR-devices, yet still function as intended for low-force applications as well. This MR-fluid device will have hysteretic behavior and velocity dependent damping that can be increased/decreased in real-time though changing of the input current to the device. It is also hypothesized that this MR-damper can produce reliable/controllable low-force damping over a relevant range of excitation frequencies (*i.e.*, those consistent with the modal properties of the small-scale structure). The scale and range of these forces produced by this device will allow it to be useful in future experiments involving wired and wireless control algorithms.

1.4 Report Organization

The next section of this report will present a literature review of the relevant history of structural control leading to the present state of the art. This literature review will present three broad categories of structural control: passive, active, and semi-active control. Examples of each category will be provided with the strengths and weaknesses indicating why semi-active control has become the preferred approach to date. A more detailed

explanation of semi-active control will be provided, due to intriguing traits suitable for future work in control and for to help the reader understand the usefulness of having this available technology for small-scale lab testing. Section 3 will focus on the technical challenges faced throughout this study. This section will include technical challenges involving damper construction and performance requirements. Also, Section 3 will discuss the designs explored during the course of this study and the reasoning for selection of a metal foam construction. Section 4 discusses how the theory, developed for magneto-rheological (MR) fluid damping forces, has to be modified to accommodate for the new design used in this study. The next section describes the experimental setup used to test both the isolated damper performance and the damper incorporated with a SDOF scale-structure. Following the experimental setup, a discussion of the collected results for this study is made. And finally Section 7 will cite the overall outcomes and conclusions of this study and offer recommendations for future work.

2 Literature Review

2.1 Structural Control

Structural control involves the provision of actuators to minimize seismic or wind excitations to protect structures and ensure occupant comfort. Properly implemented, structural control also helps to improve structural stability and dynamic performance. Structural control technologies are generally categorized into three broad groups: passive, active, and semi-active control [2]. Each respectively builds off of the shortcomings in typical devices used for structural control technologies. The state-of-the-art structural control consists of hybrid passive and active control systems as well as semi-active control devices. This section will discuss the principles behind of each type of structural control approach, give examples of each technology, describe the shortcomings associated with each, discuss which of these devices are promising for small-scale lab testing, and then describe the typical performance of commercially sold devices that might be used for comparison to the device designed for this study.

2.1.1 Passive Control

Under the passive control paradigm, a system or structure is controlled using principles of energy balance [3]. This control can be achieved through the use of elements that passively counter system response (*e.g.*, implementing a tuned mass-spring-damper system with the structure to bring the dynamic response to a desired stable response). Energy balance can also be achieved through the use of interconnecting components to provide additional paths of energy transfer and damping in the structure [3, 4]. At these interconnections passive control elements can introduced that dissipate energy in order to reduce structural response. Another way to think of passive control is to consider the two

primary components of these systems: an elastic element, to store energy and a damper, to dissipate it, neither of which impart additional energy to the structure [3, 4].

The practice of using passive control elements to dissipate the energy that is introduced into a structure as a result of earthquake excitation has been observed in buildings for over 100 years. Passive structure control was first documented in western journals by John Milne, who explained that large pendulums in Japanese Pagoda structures were used for energy dissipation [5]. The use of these pendulums was simple, relying on cantilever oscillation of the pendulum as a method of attenuating structural energy. The pendulum would strike the inside of a cylindrical hole, converting mechanical energy in the structure to some other forms [5]. Thus, the structure released energy from the system into the air and back into the ground upon earthquake excitation.

Some examples of passive control include base isolation, friction and metallic yield dampers, viscoelastic dampers, and tuned mass/liquid dampers, to dissipate energy. Each of these devices relies on a different form of energy balance. Isolation systems are passive dampers that use two components to prevent energy transfer to the controlled system. Base isolation possesses the unique blend of these two elements, damping and stiffness, provided through a mechanical system (*e.g.,* large rubber and lead bearing columns to support a structure) [2, 6]. These elements isolate the structure from ground excitations, thus limiting the energy transferred to the structure. Friction dampers and metallic yield dampers, convert mechanical energy into heat energy through friction or plastic deformation as they deform under structural or seismic loading [7]. Finally, tuned mass/liquid devices counter structural motion to balance system response (*e.g.*, story drift) under earthquake or wind loading [8].

Though these control techniques are used because of the ease of implementation, relative low cost, and their effectiveness, they do come with shortcomings. One of the chief disadvantages of passive control is that each device is calibrated to control specific excitations or behaviors (*e.g.,* tuned mass dampers that target a specific range) [9]. Out of this range, the control device may not function properly, or might fail completely [9]. Even when devices are intended to yield as a form of energy dissipation, these are other shortcomings associated passive control devices, namely fatigue and high replacement rates [2]. Due to these shortcomings newer technology have been investigated for structural control that do not require frequent replacement and are able to be effective over a broader range of conditions.

2.1.2 Active Control

Active control devices, as opposed to passive control devices, actively impart counter excitation frequencies or forces into a structure to control system response [2, 4]. Examples of active control include active mass dampers and active tuned mass dampers. Active mass dampers rely on large amounts of electricity to actuate a mass to control structural behavior based on detected structural behavior. Similarly, active tuned mass dampers use actuation methods and large power consumption to impart counter frequencies or forces onto structures.

The chief advantages active systems have over passive systems include the ability to react in short time intervals and provide a greater range of forces adequate for many different seismic excitations. Active control devices are effective at reducing story drift. Passive systems are still used for structural control, however active control systems are used to eliminate undesired disadvantages of the passive systems. The chief

disadvantages of active dampers is instability (*i.e.*, overuse/estimation of required actuation can impart more counter loads, thus imparting more energy into the system) [10], the large cost associated with first time incorporation of the systems, the external power consumption (which may be insufficiently supplied during an actual earthquake), and non-adaptability (*i.e.*, these devices require significant structure-specific design effort). These limitations have led to the exploration of control techniques that use similar principles of structural control with low electrical demands.

2.1.3 Semi-active Control

To overcome the limitations of active control, semi-active control strategies have emerged. Semi-active control devices operate under similar principles to fully-active control elements. The term semi-active, however, implies the use of less energy, and the particular way these devices create control forces indirectly. Unlike active control, semi-active control works to manipulate the stiffness or damping of a structure in real-time, thus altering the performance or behavior under excitation [2]. Even with low power consumption, the effective structural forces are very large which makes these devices particularly useful for civil structural control. Also, because of their low power requirements, semi-active control can still function in the event of a power outage, by using a backup battery. The passive nature and reliability of these devices allow for guaranteed stability, with proper equipment, and real-time structural control [4].

Examples of semi-active control devices include active variable stiffness (AVS) dampers, active bracing systems (ABS), aerodynamic appendages, piezo-ceramics or piezo-stack actuators, shape-memory alloy members, and rheological devices. AVS systems can be used to alter the full system stiffness continuously in real-time throughout

an earthquake as different frequencies are detected [11]. Active bracing systems use various bracing members, typically pre-stressed tendons linking two floors in a structure with electro-hydraulic actuator components [2]. Aerodynamic appendages are active control for wind excitation; however, these devices do not address the issue of seismic excitation of a structure [2]. Piezo-ceramics or piezo-stack actuators use small electrical charges to change length, effectively altering the stiffness of elements to achieve attenuation of vibrations [12]. Similarly, shape-memory alloys can be used to construct a part of a structure to add or release stresses, by modifying shapes of elements using electricity or heat. This shape change can lead to increased or decreased damping effects by manipulation of structural stiffness [13]. Finally, other forms of semi-active control devices have a rheological damping component, or plastic/viscous flow or solidity that can change under excitation. Rheological devices that are used for structural control are magneto- or electro-rheological fluid and elastomeric devices. The prefixes refer to the type of excitation (*e.g.*, magneto-rheological (MR) devices respond to change in magnetic flux, and electro-rheological (ER) devices respond to change in and electric field).

Because of their low-power to high-force yield, MR-dampers are popular choices for civil structural control applications. Furthermore, these devices are controllable over a broad range of frequencies and are guaranteed stable in their operation. Due to their popularity in structural control applications, MR-dampers have been selected as the subject of this study. Such devices exhibit non-linear, hysteretic behavior, leading to numerical modeling complications. These complications are independent of scale, making the low-force MR-damper a good stand in for the full-scale damper in laboratory

experiments. To provide background to understand these devices, a review of MR-damper technology is provided in the following sub-section.

2.2 MR-Dampers

This section presents an introduction to MR-damper technology including a description of MR-fluid and its behavior, as well as descriptions of a number of damper configurations based on MR principles. The effectiveness of each of these configurations for small-scale damping applications is explored as well to help justify the design decisions made over the course of this study. Finally, a brief discussion of the type of MR-damper used in this study will be provided.

2.2.1 Magneto-rheological Fluid (Ferromagnetic Fluid)

There are two main types of ferromagnetic fluid, ferrofluid and magneto-rheological (MR) fluid. The differences between the two are the particle size and concentration of iron (or ferromagnetic particles) that are suspended in a carrier fluid. Ferrofluid is composed of 5% - 10 nanometer diameter iron particles (95% carrier fluid), whereas MR-fluid uses 50 micrometer diameter iron particles that make up 10% of the volume [14-17]. Larger particle sizes and higher concentrations provide MR-fluid with stronger rheological behavior than ferrofluid [16]. Ferrofluid iron particles are lightly attracted to one another and do not strongly affect the viscosity of the fluid as a function of magnetic field. On the other hand, MR-fluid particles, being closer together, have a stronger attraction that changes as a function of change in magnetic flux. This change governs the strength of the damping effect that MR-dampers can impart to a structure [15]. MR-dampers, used in structures, can provide real-time changes in damping that are effective in controlling system responses to unwanted lateral inputs.

In addition to MR-fluids, magneto-rheological (MR) elastomers are also available options for the design and construction of dampers. MR-elastomers are based on elastomeric material impregnated with ferromagnetic particles that give them a shape-changing ability in the presence of a magnetic field [17]. The shape-change effect, similar to MR-fluid viscous change, is rapidly reversible, thus these elastomers can impart forces onto structures with real-time controllability [18, 19]. These materials are produced by curing the elastomeric material with MR-fluid additives, in the presence of a magnetic field [18]. By curing this material, iron particles (or ferromagnetic particles) are suspended in rubber, as opposed to fluid, thus the particles will not settle over time. MR-fluid dampers must periodically have their fluid remixed, whereas the chief advantage of MR-elastomers is that they retain their damping properties and composition throughout their service lives. Their chief disadvantage is the weak relationship between particle concentration and achievable damping forces of MR-elastomers. Lokander *et al.* show that maximum forces are achieved with 50% iron content as opposed to MR-fluid devices which use 10% [18]. Also, with the increased time associated with making MR-elastomers, their production cost naturally is higher. While cost is not a major concern in this study, less expensive dampers are certainly preferable to the alternative. Also, in order to achieve a better comparison to damping devices used in previous full-scale work, where MR-fluid based dampers are the dominant technology, MR-elastomers are not used in this study.

2.2.2 Different Types of MR-Dampers

Typical constituents that make up MR-fluid devices are the MR-fluid, steel pistons, steel damper housing, an electromagnetic coil (or multiple coils), and a fluid leak prevention

system (*e.g.*, either seals or an absorbent foam matrix). Steel is used for the piston and damper housing due to its high magnetic susceptibility. Since steel has high magnetic saturation properties, it can support magnetic moments, which play a role in maximum achievable force in MR-dampers. Saturation of the damper's internal magnetic circuit is a critical design property that depends on the material and geometric properties of the damper and is discussed further in the theoretical portion of this report. Three typical types of MR-dampers are used in many different mechanical and civil engineering applications: single-ended, double-ended, and sponge-type MR-dampers. These different types are presented in the following parts of this section with a description of their shortcomings related to use for small-scale test-beds.

2.2.2.1 Single-ended MR Piston Damper

Single-ended MR piston dampers use the main constituents previously described, and are arranged such that the piston moves through the MR-fluid, as seen in Figure 2.1. The electromagnetic piston, once turned on, experiences resistive forces. The forces acting on the piston can be controlled in real-time by changing the levels of applied current. The

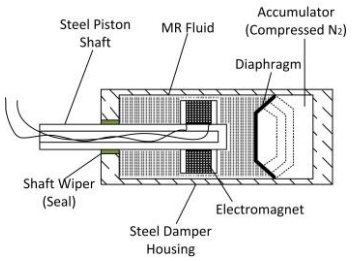

Figure 2.1: Single-ended damper and constituents

interaction between the MR-fluid to piston and MR-fluid to housing is what then imparts forces indirectly onto the retrofitted structure. This single-ended configuration is more efficient in the sense that there is only one seal used to prevent fluid leak. This seal is a

major source for undesired friction which limits the lower end of small-scale achievable forces (not an issue for commercial devices because they operate on the kN scale). Another shortcoming with constructing small-scale devices is the need for an accumulator and a diaphragm. The diaphragm folds to provide more volume for the excess fluid on the non-shaft side as the piston and electromagnetic coil moves inward, and vise-versa for the piston's outward motion. The diaphragm is stabilized by use of a compressed gas (*e.g.*, Nitrogen) acting as a pressure differential to help guide the piston in the fluid chamber. The major shortcomings associated with this design for small-scale low-force applications are that the friction forces due to the seal/piston interaction are difficult to eliminate, the difficulty in constructability for manual assembly, the use of high pressured gases, and the cantilever geometry of the piston that is difficult to support in the horizontal application intended in this project [20].

2.2.2.2 Double-ended MR Piston Damper

The next type of MR-fluid damper is a double-ended configuration as shown in Figure 2.2. Rather than using an accumulator to stabilize the piston, a double-ended piston damper employs two seals are used, one at each end, to allow the inner piston shaft to protrude from both ends of the damper. With these seals at each end support is provided

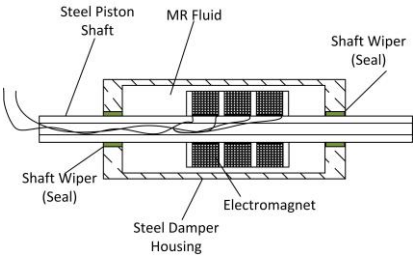

Figure 2.2: Double-ended damper and constituents

at each point, thus eliminating the need to provide cantilever support for the piston. However, this approach necessitates two seals, further degrading the minimum controllable forces of the device achievable for small-scale construction [20]. This design is more promising for horizontal application due to ease of constructability in comparison to the single-ended damper due to the better support of the piston and the elimination of the need for compressed gas or an accumulator. However, the friction created by the pair of seals needed by this damper is quite large. In fact, this friction proved to be too high for effective use in small-scale test-bed control during the course of this study. To eliminate these seals, a new approach is needed.

2.2.2.3 Sponge-type Dampers

Sponge-type dampers are used in a number of mechanical engineering applications in two forms: expulsion or extraction. Expulsion, in this context, refers to fluid being expelled out of an absorbent matrix (*e.g.,* polyurethane foam) through positive pressure. The expulsion of fluid creates shear stresses that produce to provide damping forces (Figure 2.3). Extraction refers to fluid being drawn out of an absorbent matrix, activating viscous shear forces in the damper.

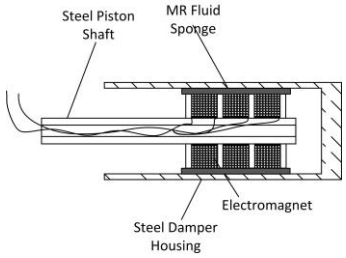

Figure 2.3: Extraction sponge-type MR-damper

The absorbent matrices within expulsion sponge type dampers are typically made of polyurethane foam. This damper type relies on the presence of the same cantilever

anchorage for horizontal applications, as is needed in single-ended devices; however it is completely seal-less. Typically, sponge-type MR dampers are single ended, but they do not require an accumulator because the sponge, or foam, guides the piston in the housing (and there is no pressure compensation required) [21]. Polyurethane foam needed for expulsion dampers is very affordable, however, it is easily torn and replacement of this matrix is very difficult in this type of damper. To avoid the tendency of the foam to tear as often, the foam thickness has to be relatively thin, thus limiting the amount of volume. Finally, the polyurethane foam surrounding the piston adds friction to the damping force, which is undesired for small-scale devices. The extraction device, shown in Figure 2.4, presents more promising attributes for the present study.

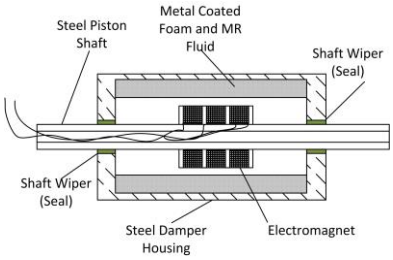

Figure 2.4: Expulsion sponge-type MR-damper

Extraction sponge-type dampers use metal coated polyurethane foam as the MR-fluid absorbent matrix. Like normal polyurethane foam, metal coated foam at small pore sizes can retain MR-fluid. As the pore size increases the ability for MR-fluid to be extracted also increases. The metal coating process has already been performed and this foam is sold commercially for purchase [22]. The poly-foam is a skeleton for the metal powder to latch on using a bonding agent. Some examples of the different types of metal foams that are available are steel composite foam, aluminum iron composite foam, aluminum foam, copper foam, and vitreous carbon foam [22]. Basic properties of metal

foams of interest for this study include absorbency and magnetic saturation. Metal foam expulsion sponge-type dampers allow for seal-less construction, however, they have not been built in such a manner. Thus, the main disadvantage to overcome for use in this study is still the friction of the seals. Another shortcoming of this configuration is delayed response time that can arise when pore sizes are small. Small pore sizes impede movement of the fluid, making it take longer to extract and change the shear forces on the piston/housing [23].

Though some shortcomings do exist in extraction sponge-type dampers when applied small-scale damping applications, if the damper is modified for a horizontal application then it can produce low forces with comparable behavior to dampers used previous work. To modify this damper to have increased response time the pore size has to be relatively large compared to that used in prior studies [22, 23]. Also, with larger pore sizes the fluid will be ineffective in the upper half of the damper housing. Thus, the foam has to be restricted to the lower half of the housing. Assuming that only the bottom portion of the fluid will be filled, and that the damper will be used exclusively in the horizontal position, seals can be eliminated from the design entirely, reducing uncontrollable friction forces.

2.2.2.4 Typical MR-damper Performance

The typical performance of MR-dampers is described using force vs. displacement and force vs. velocity curves (Figure 2.5) [24]. Additionally, magnetization curves are used to illustrate the relationships between magnetic flux, saturation, and maximum achievable damping force, useful in design. Magnetic flux increases as the current supplied to the electromagnet increases (Figure 2.6) [23]. When magnetic flux increases, the forces

achieved by the damper increase. The goal of this study is to mimic these relationships between current and magnetization, and magnetization and force (shown in Figure 2.5 and Figure 2.6).

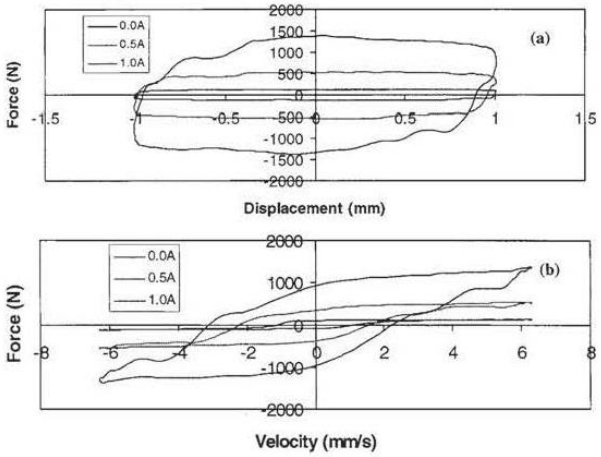

Figure 2.5: Force vs. displacement and velocity curves of LORD Corp. damper [24]

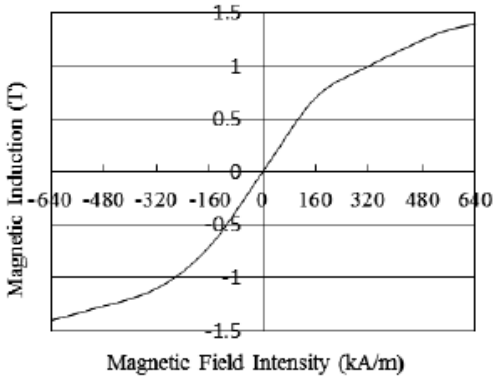

Figure 2.6: Magnetization (B-H) curve of typical MR-damper [23]

3 Technical Challenges

3.1 Constraints and Limitations for Desired Performance

Challenges encountered over the course of this study arise from the need to achieve low damping forces for the small-scale test-bed. When developing dampers for low-forces, production of damping forces dominated by magneto-rheological (MR) effects is important. Dampers that harness smart fluid properties must prevent fluid loss due to the cost associated with fluid replacement and environmental or cleanliness concerns within the structure. Techniques that are effective to prevent the leakage of fluid in full-scale dampers include vertical or angled orientation of the damper and piston shaft wipers [25]. Seals, as well as gravity, play a role in increasing uncontrollable forces produced by dampers, thus on a small-scale, friction would hinder the practical controllable range of the damper. Another issue related to building dampers is that the constituents can become damaged. The electromagnet that is an integral part of a MR-damper construction requires use of small-diameter magnet-wire (*e.g.,* 30 AWG). This wire is very delicate and can break with excess force and also fatigues easily. Also, magnet-wire has equally delicate coating (*i.e.,* to avoid the use of typical wire casing, a non-conductive coating is used) which can wear away. The likelihood of two overlapping wires with worn coating is very high because any motion between layers can wear adjacent surface coating. When both wires with worn coating touch it causes a short in the electromagnet drastically reduces the magnetic field that it can produce. Such a short will usually require that the magnet component of the piston be rebuilt entirely. These challenges can be avoided by purchasing commercially-available MR-damper technology, but both cost and technical barriers exist to adopting these components in this study. Commercially sold MR-

dampers operate on the kN scale which is not compatible with small-scale test-beds. Therefore, novel and customized design approaches are necessary to achieve the goal of a small-scale test-bed that approximates the behavior of the larger-scale systems. Scaling issues represent the most serious challenge to such a goal.

3.2 Scaling Issues

Previous work performed at the National Center for Research in Earthquake Engineering (NCREE) in Taipei, Taiwan used a 6 degree-of-freedom shake structure. Each story in this structure was scaled to be 1 meter in height with a mass of 600 kg per story. The structural parameters (*e.g.*, height, mass, stiffness, *etc.*) resulted in the modal frequencies that ranged from 0 – 25 Hz. Careful design can allow for the construction of a smaller-scale structure (with story height of 15 cm) with matching frequency-domain properties (Figure 3.1). The MR-devices used in the NCREE test-bed are sold commercially and have a 2 kN maximum force capacity. This capacity of these MR-devices is consistent with 10% of the 6 degree-of-freedom story inertial forces. The same ratio of damping to inertial forces has to be captured in small-scale damping devices that will be used in this study in order to have a meaningful comparison between control performances achieved at each scale.

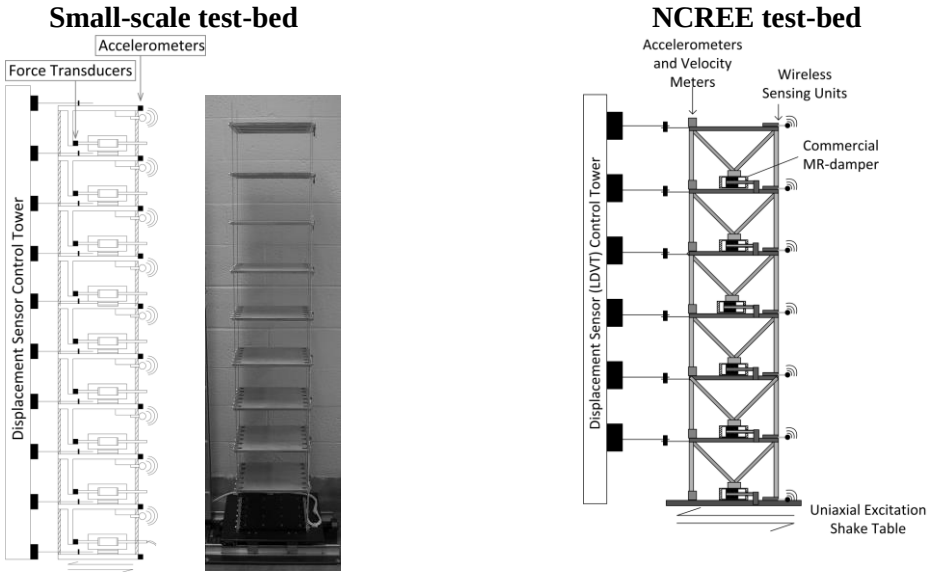

Figure 3.1: Small-scale vs. NCREE test-bed schematics

3.3 Environment/Damper Conditions

Technical challenges extend past the construction and calibration of these devices. The environment, in which the two main components exist (the electromagnet and MR-fluid), presents problems related to corrosion and leakage. Careful measures must be taken to waterproof the electromagnetic wires, such as applying two-part epoxy to the wires, as is depicted in Figure 3.2. Application of low viscosity superglue and a bond accelerant after coiling each layer can prevent wire movement and loss of magnet-wire coating, shown in Figure 3.3 as the sheen on the wires. Prevention wear of this coating will prevent short circuits and also prevent the wires from being exposed to MR-fluid. Waterproofing and the wearing of the non-conductive coating are also issues in the piston shaft, as it is hollow in order to allow the wires to escape the damper housing. As such, similar measures must be taken to ensure that MR-fluid does not leak into the piston shaft and also to prevent the wires from becoming disconnected in the core of the piston.

Figure 3.2: Epoxy coated wires

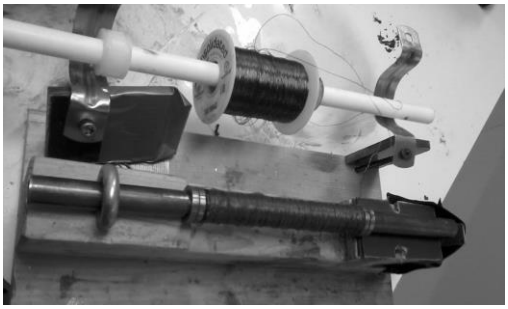

Figure 3.3: Wire wrapping station

3.4 Exploration of Two Damper Designs

With these technical challenges in as well as and the shortcomings noted earlier that are associated with each MR-fluid damper type, two designs were attempted for this study. The preliminary design is based on a double-end configuration MR-damper with seals that guide the piston and prevent fluid loss. The final design is based on an extraction sponge-type MR-damper, which does not require any extra measures that prevent fluid loss beyond the sponge itself. The expected behavior of the preliminary design was based on the optimization techniques developed by Gavin *et al.* which define the relationships between fluid volume, gap thickness, and damping force [25]. Based on the work developed by Gavin *et al.* for determining damper parameters and their relationships to desired damper forces, the initial damper design (based on the double-ended configuration) was expected to achieve an output range of 0 to 25 N forces at magnetic saturation for typical damper velocities. The actual results for the preliminary design did not reflect what was expected. The results demonstrate that the friction forces, which limit the lower end of the controllable range of the damper, are generally as high as 3.5 N, see Figure 3.4. Also, the magnetic saturation occurs at low current inputs (100 mA). Efforts aimed at ameliorating these friction forces (by the use of composite Teflon/steel

pistons) were not successful. The Teflon ends can replace weakly magnetized portions of the steel piston (*i.e.*, at the ends, far from the coil); therefore, the MR-force would not be affected, but the friction at the seals would be lowered. These efforts were able to produce modest reductions in friction forces, but not as much as was hoped.

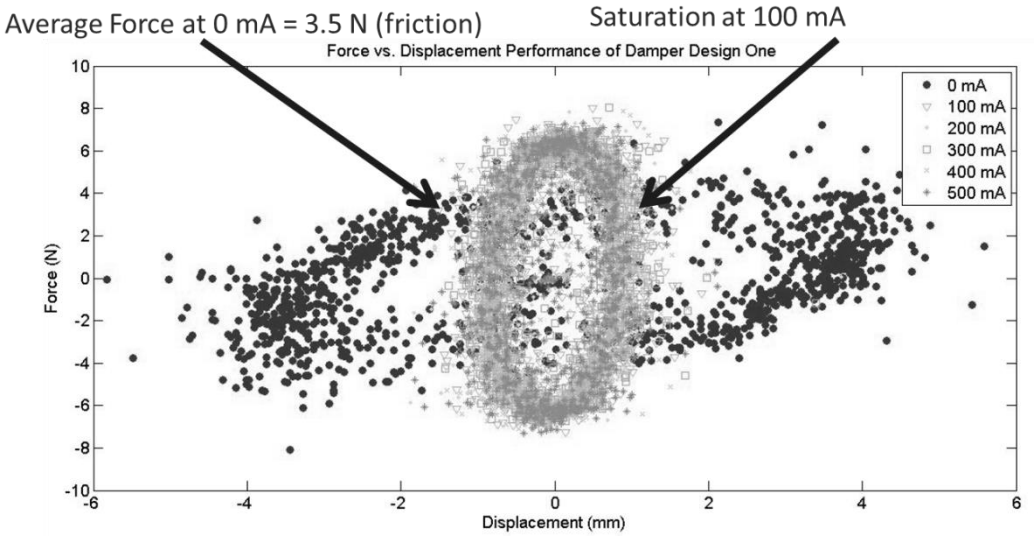

Figure 3.4: Preliminary design; double-ended piston MR-damper results

To achieve the desired low-friction behavior, it became necessary to eliminate these seals entirely. The final design uses metal foam extraction to contain the MR-fluid. Additionally, there exists a unique interaction between the MR-fluid and metal foam that serves to add extra shear stresses to the damping system for higher input currents. These alterations were made in order to meet the objectives of this study increase the controllable range on both ends of the preliminary force curve. The seal-less design provides approximately 0 N low-forces when no current is applied and greater damping forces when power (varying levels of current) is present. The design of the improved damper is presented in the following sections and the resulting behavior of the final design is reported in Section 6.

4 Theory and Methodology

4.1 Construction of Dampers

Having presented the technical challenges that are relevant to the investigation of small-scale semi-active control, this section will discuss construction issues relating to both of the designs developed for this study. In addition, dimensions and theory for both designs are presented in this section as well.

Table 4.1: Damper designs dimensions

		Units	Double-Ended	Metal Foam
Thickness of Pole	L_p	cm	0.318	0.318
Diameter of Electromagnetic Pole	D_p	cm	1.892	1.892
Length of Inductor	L_c	cm	7.620	7.620
Number of Coils	N_c	-	1	1
Number of Turns	N_t	-	2880	2880
Gap Thickness	t_g	cm	0.107	0.565
Piston Diameter	D_r	cm	1.270	1.270
Piston Inner Bore	D_{rb}	cm	0.635	0.635
Length of Piston	L_{ri}	cm	10.160	10.160
Housing Inner Diameter	D_{wb}	cm	2.105	4.763
Housing Outer Diameter	D_w	cm	2.540	5.080
Thickness of Foam	t_f	cm	-	1.270
Wire Gauge	g_{Wr}	AWG	30	30

The preliminary design was based on work by Gavin *et al.* aimed toward commercial devices [25] where friction is not an issue. The construction of the preliminary MR-damper design started with the winding of the electromagnetic coil. The work by Gavin *et al.* was aimed at optimizing the dimensions of a double-ended MR-damper. For this study, the same piston was used in each design with dimensions based on principles described by Gavin *et al.*. These dimensions are provided in Table 4.1 and shown in the schematic in Figure 4.1.

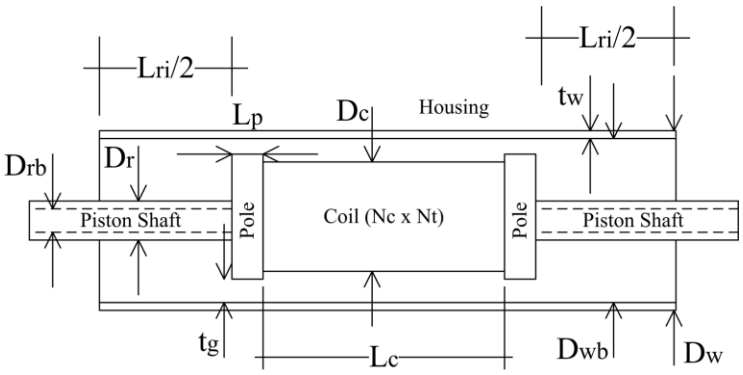

Figure 4.1: Parameters for optimization of MR-device damping forces

Using an apparatus to hold the piston in place, the coil can be wrapped by hand or by using a hand-drill. In order to generate sufficient magnetic field strength 2880 turns of the magnet-wire were necessary. Inside the damper, a magnetic circuit is formed between the piston, MR-fluid, and the outer housing. Saturation of this circuit defines the upper bound of force that the damper can provide. Each turn is represented by the wire being wrapped 360° around the piston shaft (first layer) and around the shaft and all previous rows of wires for subsequent layers. The total number of turns was determined for a coil length of 7.62 cm (3 inches), the diameter of 30 AWG wire, and the desired (theoretical) magnetic field strength. The magnetic field strength is a function of the equivalent resistance of the inductor in the electromagnet. The wire gauge impacts the resistance, proportionally.

$$i = \frac{V}{R} \qquad \text{EQN 4.1}$$

Where i is the current in the inductor, V is voltage supplied to the electromagnet, and R is the equivalent resistance of the inductor. The applied current impacts the magnetic field strength:

$$B = \mu_0 i \qquad \text{EQN 4.2}$$

Where B is the magnetic flux, or field strength, and μ_0 is the magnetic permeability. Magnetic flux in MR-dampers drives the maximum achievable damping force. Once the coil is designed with the selected wire gauge, 30 AWG in this study, and optimized turns (2880), the magnetic pole size must be optimized.

Following the procedure defined by Gavin *et al.*, both the pole thickness (L_p) and gap thickness (t_g) can be optimized to determine the effective of area the poles in order to provide optimal completion of a magnetic circuit [25]. Similarly, the piston rod outer diameter (D_r), inner diameter (D_{rb}), and rod length (L_{ri}) can be optimized. With the pole dimensions and piston info the housing length and the housing diameters had to be designed.

The housing diameter (Dw) was selected to be relatively small, to reduce the total mass of the damper (2.54 cm), and was made of steel tubing with an inner bore diameter (Dwb) of 2.105 cm (0.829 inch). Using these dimensions the total volume of MR-fluid can be determined:

$$V_{MR} = -\frac{1}{4}\pi(D_c^2 L_c + 8 * \mathrm{t_g}^2 L_p - 8 * \mathrm{t_g} D_{\mathrm{wb}} L_p + D_r^2 L_{\mathrm{ri}} - D_{\mathrm{wb}}^2 (L_c + L_{\mathrm{ri}})) \qquad \text{EQN 4.3}$$

By setting L_p and D_c equal, V_{MR} can be simplified to:

$$V_{MR} = -\frac{1}{4}\pi(D_c^2 (L_c + 2L_p) + D_r^2 L_{\mathrm{ri}} - D_{\mathrm{wb}}^2 (L_c + 2L_p + L_{\mathrm{ri}})) \qquad \text{EQN 4.4}$$

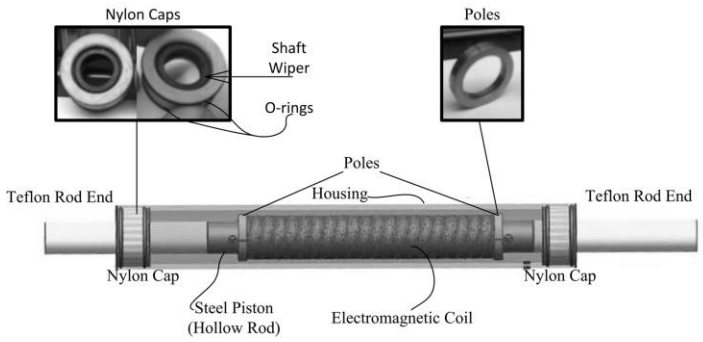

Figure 4.2: Preliminary design constituents

This fluid volume is held inside of the housing by nylon caps sealed with o-rings and shaft wipers, as seen in Figure 4.2. With all of the constituent dimensions and the fluid volume known, construction of the preliminary damper can begin. Using the steel housing with grooves on the ends to match the o-ring thickness for a proper water-tight seal (refer to Appendix A CAD drawings for more detail), one can fit a nylon cap assembly into one end of the housing. Next, the piston may be placed into the shaft wiper in the nylon cap assembly. With a water-tight seal around the piston and housing established, MR-fluid can be added. To finish to assembly, the seal at the other end is made using a second nylon cap assembly.

With the preliminary design built and tested, excess friction forces were observed (reported in Section 3), a second design was devised. This design uses the same electromagnet and relies on a fluid absorbent matrix to prevent spillage of MR-fluid, not seals. Without seals, the total volume of fluid used in this design will decrease, and can no longer be represented by the previous equations. In this configuration, the metal foam dimensions constrain the total amount of fluid that can be used in the damper housing. As discussed in the literature review of this report, many different types of metal foam exist, but aluminum coated foam was chosen for this study. This decision was made because of

availability, cost, and low magnetism of aluminum coated foam. Low magnetization or magnetism of the foam is desired because it would allow for MR-fluid to be extracted in the presence of a magnetic field. If the metal foam matrix was ferromagnetic it would attract MR-fluid suspended iron particles magnetically, leading to delays in damper performance. Due to the new configuration and the new definition for volume, a larger conduit diameter was chosen to compensate for lost volume (5.08 cm). The thickness of foam was then chosen to be 1.27 cm (0.5 inches) in order to provide enough fluid volume to achieve the higher forces sought for the test-bed structure. The schematic for this design and a photograph of the interior of the housing are shown in Figures 4.3 and 4.4, respectively.

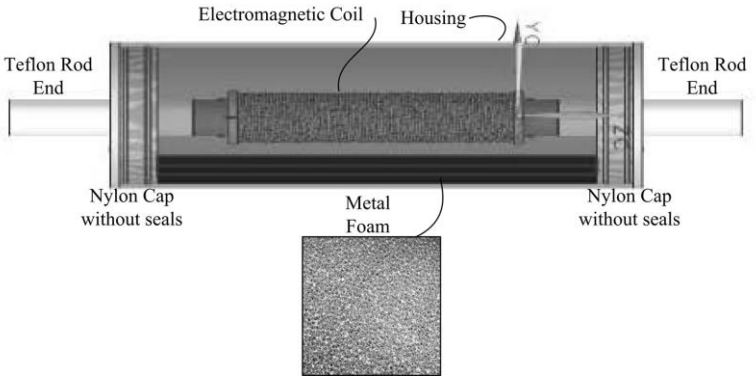

Figure 4.3: Final design constituents

Figure 4.4: Final design interior

Knowing the dimensions and the percent porosity of the foam (80%) the volume of the MR-fluid can be calculated using:

$$V_{MR} = (L_h((R_b)^2 * \text{ArcCos}\left[\frac{R_b - h}{R_b}\right] - (R_{wb} - h)\sqrt{2 * R_b * h - h^2})) * P_v \qquad \text{EQN 4.5}$$

Where L_h is the length of the housing, R_b is the inner radius of the housing ($D_{wb}/2$), h is the height of fluid, and P_v is the percent porosity. The advantages of this

design are that the fluid volume to piston ratio can be calibrated to achieve a desired level of force and that the fluid will be contained in the housing using the absorbent foam matrix, rather than seals. Full details of the final damper design can be found in Appendix A.

4.2 Effective Annular Volume

Due to the strong relationship that exists between MR-fluid volume and achievable for estimating damping force the reduced MR-fluid volume must be considered [25]. To do so an effect annular volume is approximated. In commercially-sold MR-fluid dampers, MR-fluid surrounds the piston on all sides, annularly. This is not the case with the metal foam matrix device used in this study; however, at some diameter the volume in the foam can be projected to an effective annular volume (Figure 4.5), which is done by calculating the volume of fluid in the foam matrix, by equating the gap thickness to the distance between the magnetic poles and the housing, and determining α and β as follows.

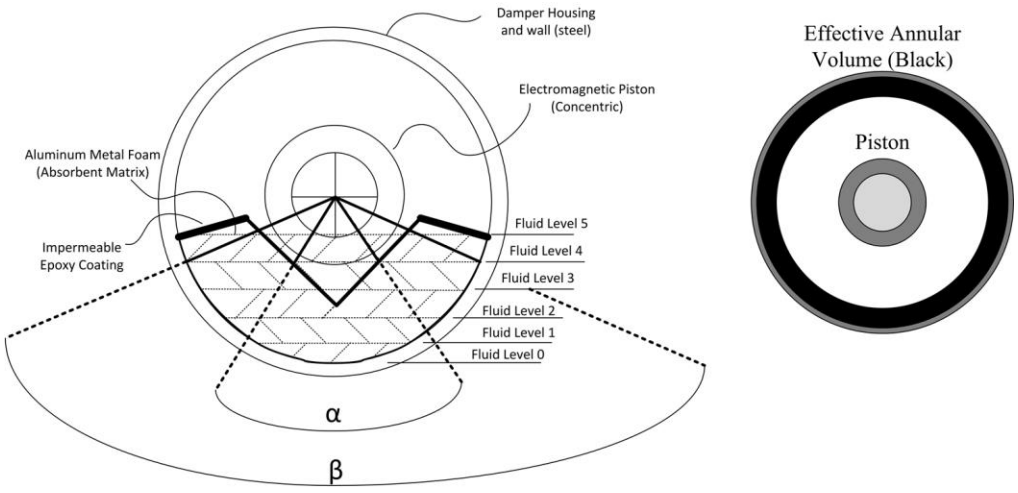

Figure 4.5: Parameters for estimating MR-fluid effective annular volume

The process for obtaining the effective annular volume can be simplified to two parameters, α and β. Where α is the effective angle of the MR-fluid acting between the

damper piston and the outside of the metal foam. Note that α reduces to zero if the fluid level is less than the foam thickness in Figure 4.5. Therefore, the effective damping force range exists between a fluid level equal to the foam thickness and a level greater than the foam thickness. The parameter β is the effective angle of MR-fluid acting on the damper housing, and should not be strongly effected by fluid level if α is constrained. With these parameters a factor is developed to calculate damping force using an effective annular volume. This effective annular volume factor is calculated by:

$$\beta = \frac{360° * \sqrt{-h * (h - 2 * R)} * (h - R) + R^2 * Cos^{-1}(1 - \frac{h}{R})}{\pi * R^2} \quad \text{EQN 4.6}$$

$$\alpha = \frac{360° * \left((h - R_p)\sqrt{-h^2 + D_{wb}h + 2t_f h} + {R_p}^2 Cos^{-1}\left(\frac{-h + \frac{D_{wb}}{2}}{R_p} \right) \right)}{\pi * {R_p}^2} \quad \text{EQN 4.7}$$

$$V_{fh} \simeq \pi \left((\frac{D_{\mathrm{wb}}}{2}) - \left(\frac{\mathrm{D_p}}{2} \right)^2 \right) \quad \text{EQN 4.8}$$

$$V_{eff} = \frac{1}{2 * 360°} \pi (\mathrm{t_f} - \mathrm{t}_g)(\alpha + \beta)° (\mathrm{t_f} + \mathrm{t_g} - D_{\mathrm{wb}}) \quad \text{EQN 4.9}$$

$$F_{mrf} = \frac{\pi^2 (\mathrm{t_f} - \mathrm{t_g})(\alpha + \beta)° (\mathrm{t_f} + \mathrm{t_g} - D_{\mathrm{wb}})}{360° * \left((\frac{D_{\mathrm{wb}}}{2})^2 - (\frac{\mathrm{D_p}}{2})^2 \right)} \quad \text{EQN 4.10}$$

In this set of equations, V_{fh} is the simplified volume if the entire damper housing is full. V_{eff} is the effective volume of fluid acting on the electromagnetic coil. Finally, F_{mrf} is the factor that can be used to modify the annular volume equations to match the new design configuration without an annular volume.

4.3 Theoretical Magnetization and Forces

The theoretical magnetization and damping forces build on the theory behind the effective annular volume. Every MR-fluid device has what is known as an MR-valve structure. The MR-valve structure describes the Kirchhoff magnetic circuit as shown in

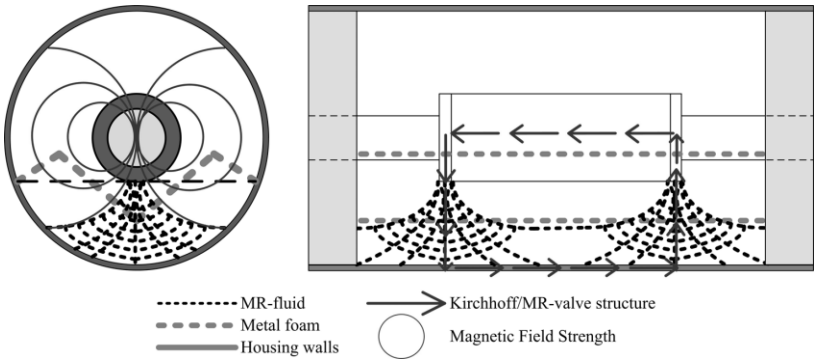

Figure 4.6: Magnetic field and fluid draw; magnetic circuit links

Figure 4.6 (depicted by arrows in the right image). The damping force associated with a metal foam damper exists within one half of the housing, depending on the specific configuration. Typically with an actual annular volume, as opposed to an effective annular volume, the Kirchhoff magnetic circuit is completed on both halves of the housing [25, 26]. The magnetic circuit is completed through the steel components of the piston and housing as well as the MR-fluid. In between piston and housing the MR-fluid and metal foam have lower magnetic permeability, therefore it is harder to complete the circuit. Low permeability greatly impacts the maximum force achieved by the damper. Therefore, the theory behind a new magnetization curve of the extraction sponge-type MR-damper design has to be developed. This can be done using the following equations for B (magnetic flux) and H (magnetizing field).

$$B = \frac{p_h}{A} \qquad \text{EQN 4.11}$$

$$H = (k_{St} * e^{k_{St} * B^2}) * B \qquad \text{EQN 4.12}$$

Where p_h is the magnetic flux conservation coefficient, A is the cross-sectional area associated with the material (*e.g.*, effective area of MR-fluid acting on the poles), and k_{St} is the steel B-H curve coefficient. Figure 4.7 depicts the different magnetization curves for the various constituents affecting the damping force (*i.e.*, steel, MR-fluid, and

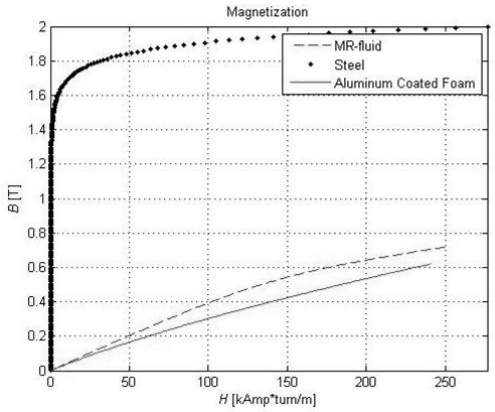

Figure 4.7: Magnetization curves of MR-fluid, steel, and aluminum coated foam

aluminum foam). From Figure 4.7 the steel B-H curve coefficient can be determined for the linear range in which the damper will operate. These magnetization curves are proportional to the maximum achievable damping forces if all components were made solely each individual material separately. Taking the steel B-H curve, for example, if everything was made of steel, the damping force would be very high. Likewise, if the entire damper was made of aluminum (including the MR-fluid) the damping force would be very low. Therefore, another process developed by Gavin *et al.* can be used to simplify these three constituents, and the effective area acting toward the magnetic circuit, into one magnetization curve [25]. With the new B-H magnetic curve that involves steel components, MR-fluid, and aluminum foam, the following equations can be used to

determine the maximum theoretical damping force within the range of operational velocities.

$$Q = \frac{v_p * V_{eff}}{L_h} \quad \text{EQN 4.13}$$

$$\Delta p_N = \frac{24 * Q * \eta * L_p}{\pi(D_p + t_g) * {t_g}^3} \quad \text{EQN 4.14}$$

$$p = 160 * \frac{B}{t_g} + \Delta p_N \quad \text{EQN 4.15}$$

$$F = p * \frac{V_{eff}}{L_h} \quad \text{EQN 4.16}$$

4.4 Role of Metal Foam and Expected Interaction with MR-fluid

To summarize the behavior of the damper with added metal foam, primarily it is used hold the MR-fluid. However, upon magnetization the fluid will become partially extracted from the foam. Once extracted, the MR-fluid bridges the gap between the damper housing and the piston, thus completing the magnetic circuit and the MR-fluid can generate the shear stresses in the damper. Additionally, it is expected that the interaction between the fluid and metal foam will behave, effectively, like friction (thus, "effective friction" in future usages). As such, additional controllable forces will be achieved as a result of having this metal foam in the housing. With effective friction added to the damping force there is room for future work to provide additional controllable forces within the damper.

4.5 Output of Theoretical Model

Overall, with the additions to the theory by Gavin *et al.* a numerical model was generated in MATLAB. In Figure 4.8, peak force versus flux density is plotted neglecting effective friction. In Figure 4.9, peak force versus input current is shown. These results

show that the maximum theoretical damping force within operational velocities is approximately 4 N based on the magnetic saturation limit of the magnetic circuit. Saturation is the point at which no additional damping force can be achieved with additional current or magnetic field strength. The saturation magnetic flux is 0.419 Tesla and the saturation current is 476 mA. (Figure 4.10). It will be shown, experimentally, that neglecting the effective friction forces provided by the metal foam, will tend to considerably underestimate the damping force that is achievable by the damper. The experimental procedure used to demonstrate this fact is presented in the next section.

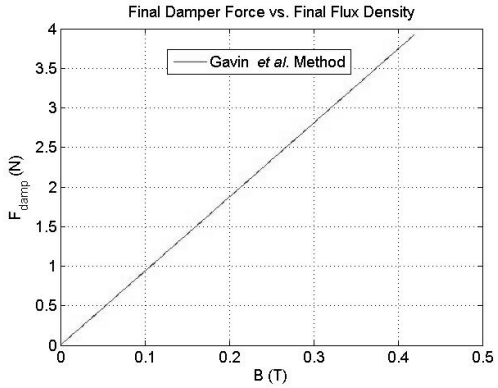

Figure 4.8: Theoretical damping force vs. magnetic flux

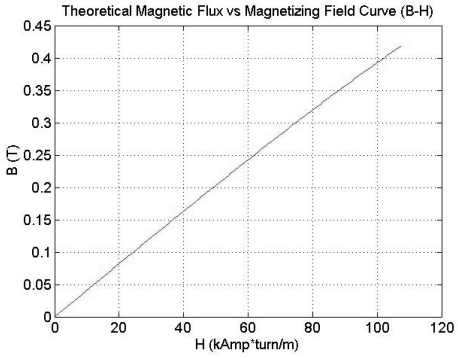

Figure 4.9: Theoretical magnetic saturation curve

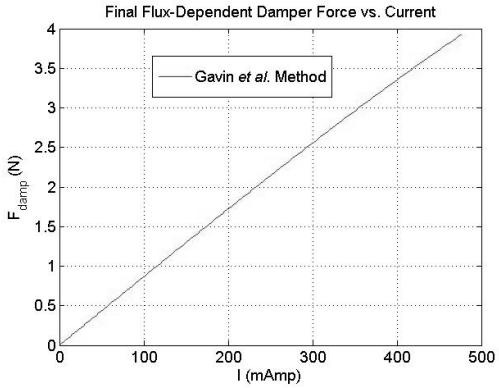

Figure 4.10: Theoretical damping force vs. current

5 Experimental Setup

This section describes the two experimental setups and testing equipment used for collecting data with the extraction sponge-type MR-damper prototype. The first setup was designed to explore the damping properties of the MR-damper isolated from the effects of any structure. The second setup was designed to study the behavior of the damper incorporated with the elements of a single-degree-of-freedom (SDOF) small-scale structure. Respectively these test setups are used to validate the basic performance requirements of the damper (*e.g.*, force range, behavior, *etc.*) for future work in wired/wireless control, and to show the damping behavior with structural influence.

5.1 Testing Equipment

Data is acquired using sensors and a National Instruments NI PXIe-1071 chassis, which was chosen due to its speed, channel count, and its ability to serve as the control server in with future wired control experiments using the MR-damper. The associated data-collection software used was LabVIEW. To power the damper a U3606A Multimeter DC Power Supply was used with hi-polar outputs of up to 1.0 A current and 30 V voltage. This current range is adequate to power the damper prototype and is sufficient for comparison to commercial devices. Other equipment chosen for this study include: the small-scale shake table test-bed (Quanser Shake Table II system controlled by Mathworks Simulink and a proprietary real-time control package, QUARC, made by Quanser) and a Piezotronics sensor signal conditioner and sensor power supply. Specific sensors used depend on the experimental setup and are described in those sections.

5.2 Isolated Damper Setup

The isolated damper setup was used to determine the maximum damping coefficients and forces achievable by the MR-damper. In this test setup a Quanser Shake Table II was used to provide uniaxial seismic excitation. The sensors chosen for this project were a PCB Piezotronics accelerometer and force transducer, model #'s 333B32 and 208C01, respectively. The piston was mounted to a rigid column mounted to the floor of the lab. This configuration limited the use of displacement sensors, therefore accelerometers were used to obtain displacement and velocity. These sensors were configured as seen in Figure 5.1. Here it can be seen that the force transducer was installed in-line with the piston and the rigid column in order to detect resistive (or damping) forces. Additionally, an accelerometer was placed on the shake table to measure ground/housing displacement.

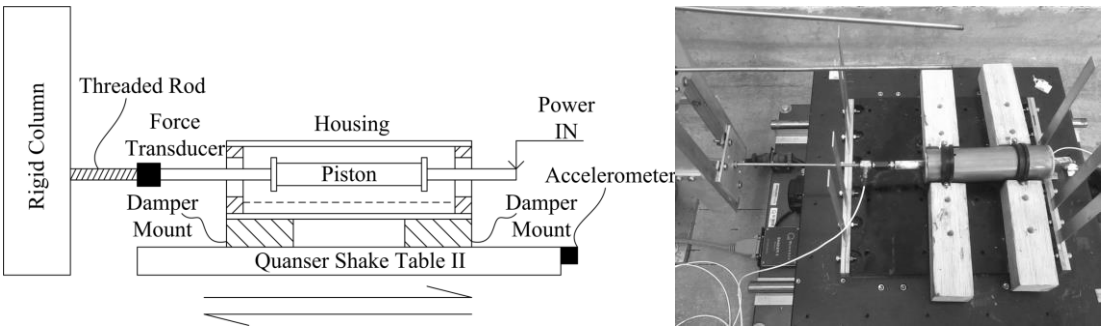

Figure 5.1: Isolated damper setup and sensor placement

With the force transducer data, force vs. velocity and force vs. displacement plots can be generated with varying inputs. Sine wave inputs of varying frequencies were used throughout this study. This overall setup was used for the prototype damper with aluminum coated foam. In addition, a second damper with matching dimensions, but without foam was tested as well. By removing the foam and replacing it with the same MR-fluid level, the anticipated effective friction could be characterized. The behavior of

the damper at varying fluid levels, various damper input currents, and operational frequencies were tested and recorded.

5.3 Damper *In situ* Setup

The purpose of the single-degree-of-freedom (SDOF), or *in situ*, study is to determine the behavior of the damper in the environment that it is designed for. Also, the resonant frequency will have potentially damaging effects on the structure if the damper cannot alter the dynamic properties of the system of that frequency. Figure 5.2 shows the SDOF model describing the behavior of the bare test structure without damping provided by the MR-fluid damper.

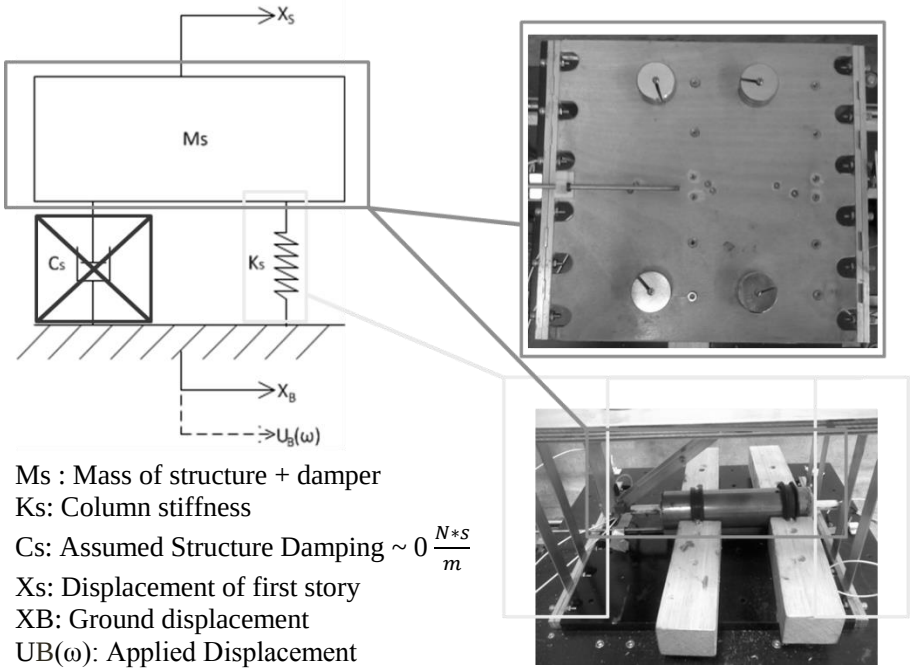

- Ms : Mass of structure + damper
- Ks: Column stiffness
- Cs: Assumed Structure Damping ~ 0 $\frac{N*s}{m}$
- Xs: Displacement of first story
- XB: Ground displacement
- UB(ω): Applied Displacement

Figure 5.2: SDOF model of a small-scale test-bed without damping

Governed by this model, structural dynamics can be used to find the resonant frequency of the SDOF structure using the following equations:

$$I = \frac{bh^3}{12} * n_{col} \quad \text{EQN 5.1}$$

$$Ks = \frac{3EI}{L^3} \quad \text{EQN 5.2}$$

$$\omega_n = \sqrt{\frac{k}{Ms}} \quad \text{EQN 5.3}$$

$$F_n = \frac{\omega_n}{2\pi} \quad \text{EQN 5.4}$$

In these equations E is the modulus of elasticity (for this study E of Aluminum), I is the area moment of inertia of the columns, n_{col} is the number of columns (8 for this study), and M_S is the Mass of the structure, piston, and mounting bracket. Also, K_S is the column stiffness, L is the column length (15 cm), ω_n is the natural frequency in rad/sec, and F_n is the natural frequency in Hz. With these properties defined, the natural frequency was found to be 6 Hz. As such, the excitation range defined for this experiment was set to 0-8 Hz to demonstrate the efficacy of the damper prototype over a frequency range that includes resonance of the structure.

In addition to the accelerometers and force transducers described in 5.2 displacement sensors (MTS C-Series Core Linear Position Sensors) were used to characterize the performance of the damper as part of a SDOF controller. Damper behavior was tested over a range of relevant input currents (0 – 700 mA) and ground motion frequencies (0 – 8 Hz). Figure 5.3 shows the sensor placement, including the accelerometers and displacement sensors located on each level of the SDOF small-scale structure. A photograph is also provided in Figure 5.4 that shows the plan view of the structure and how the displacement sensor (left) and accelerometer (right) are aligned to the center of the test-bed. Also, there is a force transducer located between the damper

piston and upper story to measure damping force, depicted in Figure 5.3 and shown in Figure 5.6. This configuration, using a mounting bracket (Figure 5.5), adds an inertial force to the force transducer provided by the damper piston.

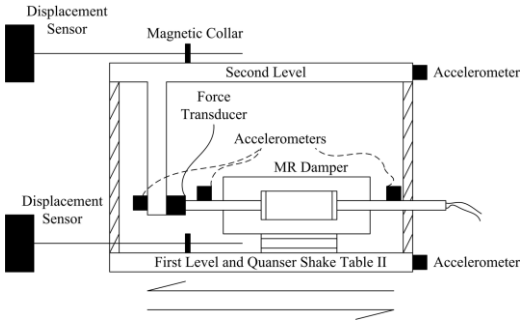

Figure 5.3: Sensor placement *in situ*

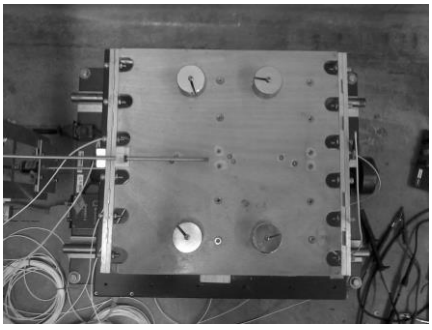

Figure 5.4: Plan view of structure

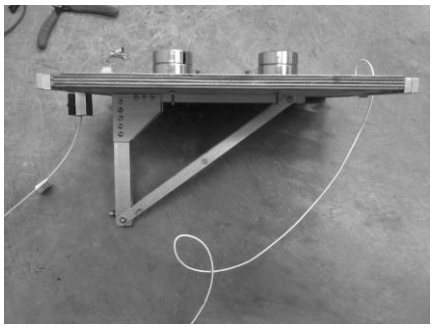

Figure 5.5: Damper mounting bracket

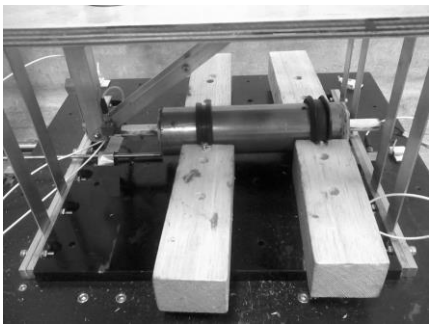

Figure 5.6: Damper *in situ* with sensors

The force transducer can be used to get full system forces in this setup. In this setup, the force transducer measures both shear forces transmitted through the MR-fluid from the piston to the housing, as well as the inertial forces associated with the piston. An additional accelerometer connected to the free end of the piston provides a means of estimating and correcting for the damper inertial force (Figure 5.3). The damping force is calculated using the following equation:

$$F_d = F_{\text{tran}} - F_p \qquad \text{EQN 5.1}$$

Where F_d is the damping force achieved by the MR-damper, F_{tran} is the force transducer data, and F_p is the inertial force of the piston equal to its mass times its absolute acceleration. The displacement from each sensor is then used in the calculation of relative floor displacement/drift:

$$\delta_R = \delta_2 - \delta_g \qquad \text{EQN 5.2}$$

Where δ_R is the relative displacement required for the force vs. displacement plots (also necessary for calculating relative velocity), δ_2 is the displacement of floor two and δ_g is the displacement of the base. Finally, differentiation of the displacement data using forward differentiation generates the relative velocity (v_R):

$$v_R(\mathrm{t}) = \frac{\partial \delta_R(t)}{\partial t} = \frac{\delta_R(t + \Delta\mathrm{t}) - \delta_R(t)}{\Delta\mathrm{t}} \qquad \text{EQN 5.3}$$

5.4 Data Processing

Data was processed using MATLAB. Data processing involved a basic filtering process. A digital band-pass filter was used, using MATLAB built-in butterworth second order low-pass filter and Savitzky–Golay second order high-pass filter. The band-pass filter was used to remove noise captured by sensors from the shaking environment as well as sensor and circuit noise. After filtering the data it was de-trended (*i.e.,* subtract out the mean, or sensor offset, and a trending regressive line from the data). Finally, the data was averaged using smooth.m, another built-in command in MATLAB that is used to smooth out any remaining noise. In the unfiltered band of unfiltered frequencies, the smooth command averages specified windows (*i.e.,* it uses consecutive data points, high and low, to find the mean value that can describe the trend the filtered data suggests).

6 Results and Discussion

This section presents the results gathered from data collected to characterize the behavior of the extraction sponge-type MR-fluid damper in the two previously described experimental setups. These tests were performed to verify that this device behaves like a large-scale commercial MR-device. The tests in each setup consisted of varying currents supplied to the damper 0-700 mA. This was to test the damper's magnetic saturation limit to compare with what was determined theoretically. Additionally, since the resonant frequency of SDOF was found to be 6 Hz, both setups had to accommodate excitation frequencies ranging from 0-8 Hz. Also, because damping force is a function of velocity, tests were performed to see the hysteretic behavior of this device with respect to force, velocity, and displacement. With the set of frequency varying tests, the presence of frequency independent damping was checked in the damper. A final test was performed to verify the effect MR-fluid level has on damping force (fluid levels ranging from 0 – 1.5875 cm in 0.3175 cm increments).

6.1 Results of Damper Isolated from SDOF Scale-Structure

The following figures show the data collected when the damper was isolated from a structure. The damper housing was excited in uniaxial motion with 0-8 Hz sine waves. The forces are depicted in Figures 6.1 (versus displacement) and 6.2 (versus velocity), and show the general hysteretic behavior of the prototype device. The maximum force from these two plots is observed to be 12 N at 55 mm/s which compared to the velocity independent theoretical force of 4 N, demonstrates that the peak force can be tripled when effective friction is considered. Damping increases as a function of velocity. Therefore in Figure 6.2 there is an observable trend between force and velocity. To check

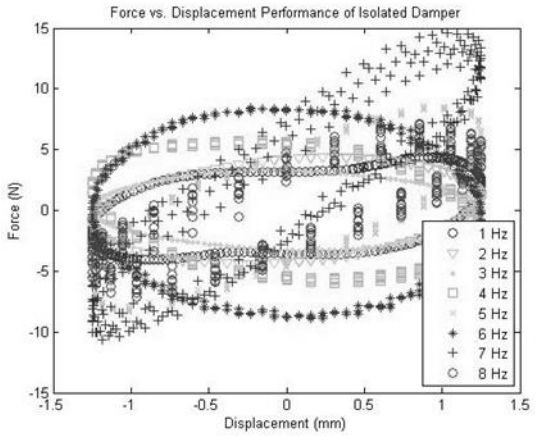

Figure 6.1: Force vs. displacement of the isolated damper with foam

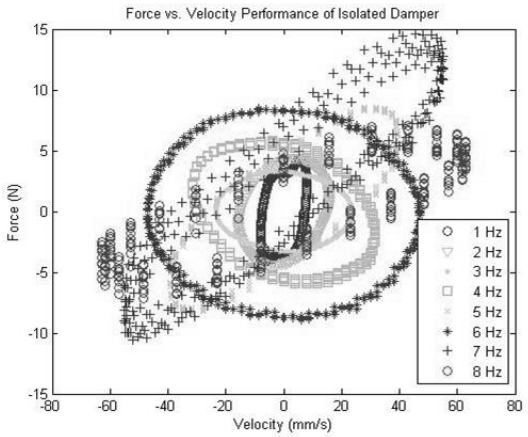

Figure 6.2: Force vs. velocity of the isolated damper with foam

if the damping coefficient is independent from the excitation frequency, the velocity at each peak force can be factored out, leaving units of N-s/mm or damping (*e.g.*, at 6 Hz frequency the max velocity is 55 mm/s and the force is 12 N, so the damping is 12N / 55 mm/s or 0.218 N-s/mm). The trend, by dividing all maximum forces by their

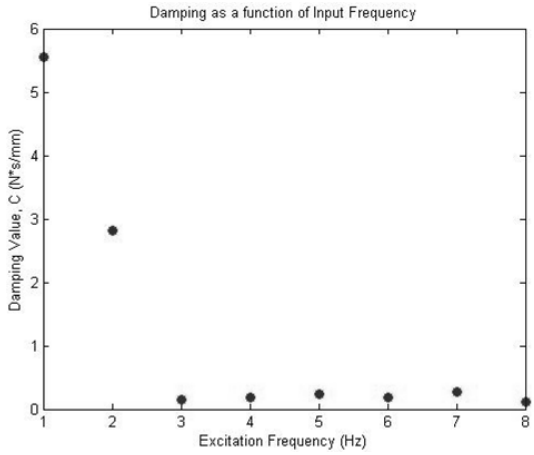

Figure 6.3: Frequency independent damping of the isolated damper

corresponding velocities is plotted in Figure 6.3. This figure shows that the damping coefficient is more or less the same from 3 Hz to 8 Hz. The high damping value at low frequencies is associated with high signal/noise ratio in that the velocity measurements in

these frequency ranges were quite small and the measurements were rather noisy. Therefore, there is an indication that the damping coefficient in the isolated setup is frequency independent.

The damper was tested with foam in the housing, but modeled without. Therefore a study was conducted into characterizing the effect of the foam by removing the foam and filling the housing with equal height of fluid. Under these conditions, force versus displacement and force versus velocity plots have been generated (Figures 6.4 and 6.5) which show a general damping force of approximately 4 N over the range of operational velocities, which is consistent with the predicted theoretical force. Therefore, the difference can be associated to the shear reaction (effective friction) between the MR-fluid and metal foam.

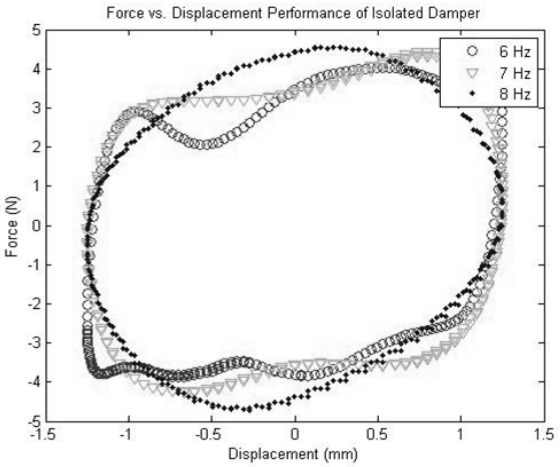

Figure 6.4: Force vs. displacement of the isolated damper without foam

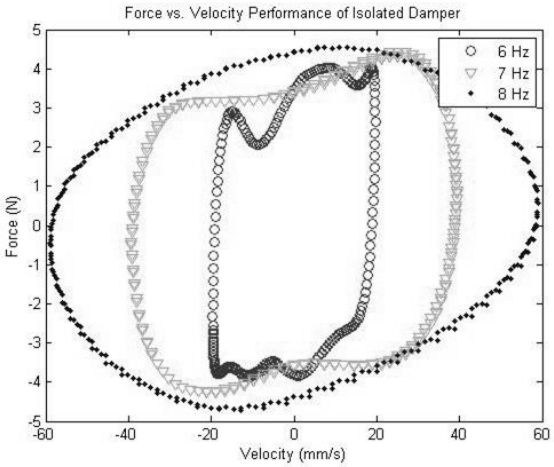

Figure 6.5: Force vs. velocity of the isolated damper without foam

6.2 Results of Damper Integrated with SDOF Scale-Structure

In the case where the damper was integrated with the single-degree-of-freedom (SDOF) structure, damping forces are shown in Figure 6.6 and Figure 6.7. These plots show hysteretic/bi-linear behavior with force magnitudes that vary with input current. In these

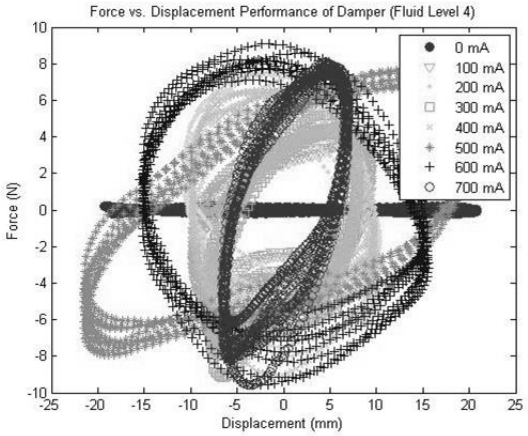

Figure 6.6: Force vs. displacement of the damper *in situ*; low frequencies

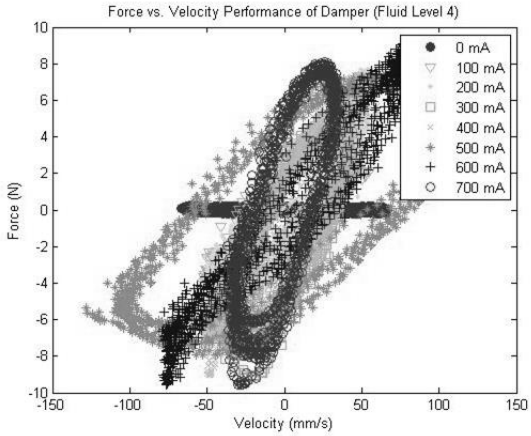

Figure 6.7: Force vs. velocity of the damper *in situ*; low frequencies

plots one can see that saturation is occurring at about 500 mA, consistent with the numerical model and theory described in Section 4. A maximum damping force of 8.64 N (Figures 6.6 and 6.7) was achieved at 50 mm/s (Figure 6.7) at a 5 Hz excitation frequency, just below the 6 Hz resonant frequency of the SDOF structure. Therefore, the damping coefficient of the MR-fluid device *in situ* is 172.8 N-s/m. This peak is lower than the damping provided in an isolated scenario due to feedback between the damper and the structure.

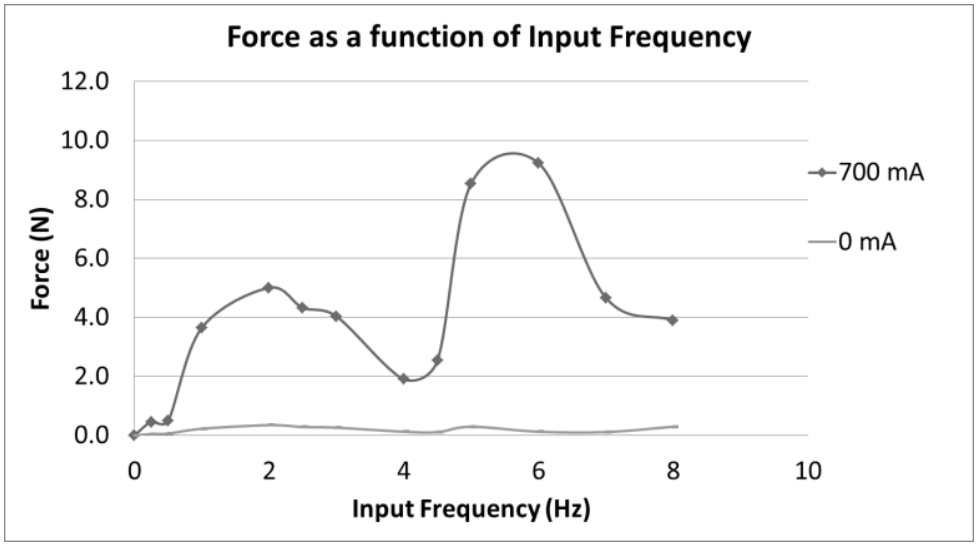

Figure 6.8: Frequency dependence when damper is integrated with structure

Figure 6.8 shows that *in situ* there is a relationship between damping force and frequency, not observed when the damper was isolated. When isolated the damping force increases with frequency increase (due to increases in velocity associated with frequency increases), but in this is not the case when integrated with the structure. Therefore, there is a dependency on the structural interaction and the measured damping force making the behavior of the isolated damper difficult to measure in this configuration. However, this configuration does demonstrate that the damping forces provided by the damper are effective at the resonant frequencies of the structure. In the two figures, Figures 6.9 and 6.10, forces are plotted for the damper at and above resonance of the structure. The maximum damping force was still observed to be around 12 N at 55 mm/s, consistent with the isolated damper; however, the data after averaging is still quite variable. This variability further illustrates the difficulty in characterizing the damper behavior *in situ*. Some key information to take away from this portion of the study can not only be represented in the time-domain, but also in the frequency domain. In the frequency

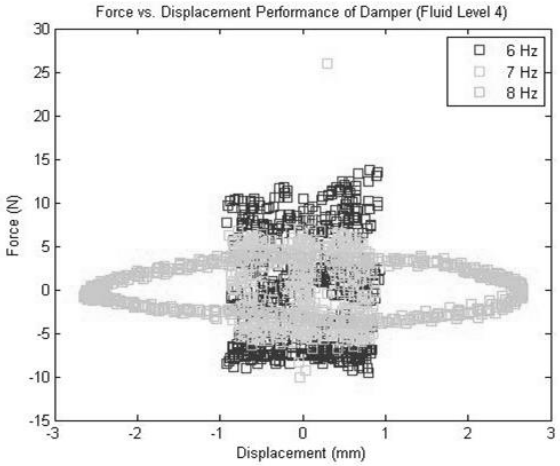

Figure 6.9: Force vs. displacement of the damper *in situ*; high frequencies

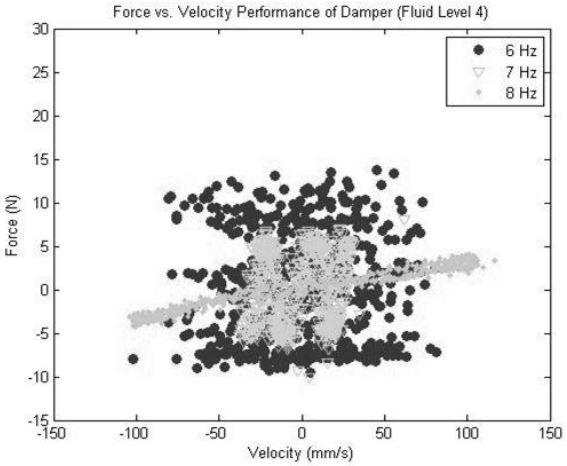

Figure 6.10: Force vs. velocity of the damper *in situ*; high frequencies

domain it can be observed how displacement or drift is reduced with increased damping. Also, in the frequency domain one can observe the increase in damping force and the ability for the damper to capture all excitation frequencies. As can be seen in Figures 6.11 and 6.12, these two relationships are shown.

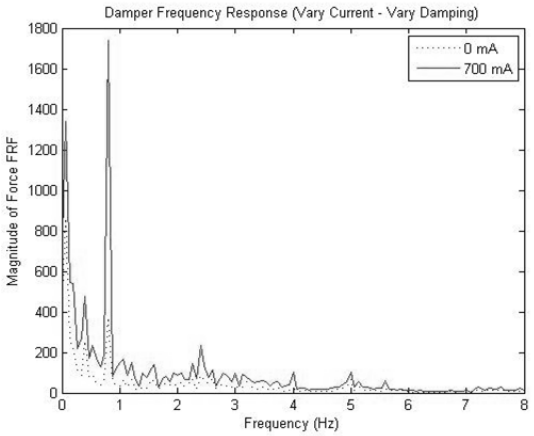

Figure 6.11: Damping force in frequency domain

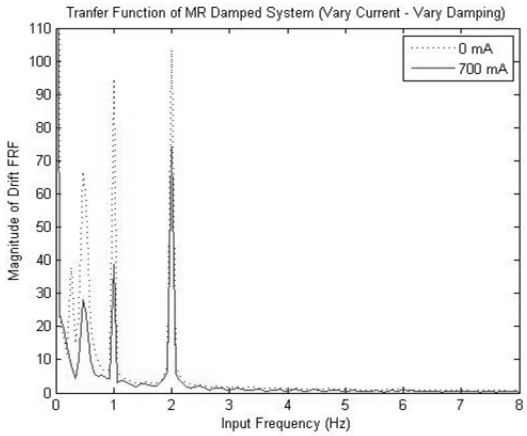

Figure 6.12: Drift reduction in frequency domain

One final investigation was performed for this study and this was to determine the relationship between fluid height and damping force. Figure 6.13, plots the force

generated by the extraction sponge-type MR-fluid damper with varying levels of fluid at a single excitation frequency (5 Hz) and at the minimum and maximum allowable currents. This plot shows that an optimal level of fluid is likely to exist as 1.27 cm (which is the same as the thickness of the foam) based on the diminished increase in force above this level. Beyond this height the variance in outputs increases as well due to sloshing and spilling of MR-fluid from the housing.

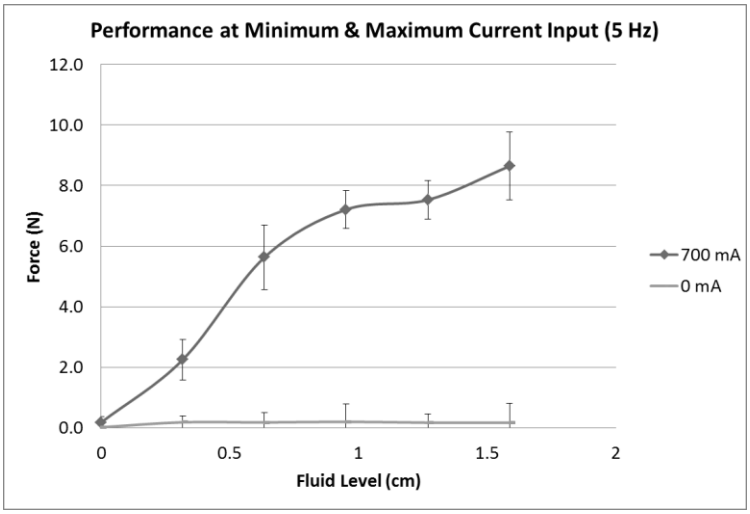

Figure 6.13: Effect of fluid level on damping force at 5 Hz excitation

7 Conclusions and Future Work

7.1 Conclusions

Semi-active damping devices are of particular interest in civil engineering, however modeling of these devices presents several difficulties. To harness the control techniques of semi-active devices for small-scale testing it is required to test them extensively. In this study, to enable the development of a small-scale test-bed for semi-active control devices, two magneto-rheological (MR) damper designs were investigated. These semi-active devices were chosen to be MR-fluid dampers for consistencies with full-scale civil structural control applications. Due to design limitations discovered in the preliminary, double-ended MR-damper design, a final design was chosen to be an extraction sponge-type MR-device. This study has shown that a small-scale device can be made to have comparable attributes to large-scale commercial devices. These attributes include hysteretic forces and an adequate magnetic saturation curve for matching the controllable range of the damping forces to the test-bed structure. Also, the damper demonstrated the ability to damp multiple input frequencies of a SDOF test-bed structure at the scale of interest.

The overall maximum damping coefficient of this damper was found to be adequate. This performance was observed when the damper was isolated from the SDOF test-bed. This force differed from previously established theoretical forces because of the existence of effective friction, or shear reactions, between the MR-fluid and the metal foam. It was found that the effective friction force was significant, as much as 200% of the bare housing (theoretical) value. Though the effective friction was significant, the theoretical and experimental magnetic saturation limits matched. A separate test was

performed to demonstrate the theoretical force does match experimental data when the foam is removed. The damper was integrated with the structure and showed comparable behavior to commercial devices in literature. Finally, a study was conducted to find the optimal level of MR-fluid; it was found that the optimal level was equal to the foam thickness of within the housing.

7.2 Future Work

Since a relationship was found between the foam thickness and maximum force in the damper, future work should include optimizing the porous media thickness and density. In addition, testing should be conducted on a multi-story scale test-bed structure. Investigation and derivation of an operational model (*e.g.,* Bouc-Wen control model) for this damper should be performed for use in real-time control applications. Finally, for comparison to full-scale experiments, the small-scale structure with implemented metal foam dampers should be tested for effectiveness under simulated historic ground records using a real-time controller.

8 References

1. Wang, Y., Swartz, R.A., Lynch, J.P., Law, K.H., Lu, K.-C., and Loh, C.-H., *Decentralized civil structural control using real-time wireless sensing and embedded computing.* Smart Structures and Systems, 2007. **3**(3): p. 321-340.
2. Spencer, B.F., Jr. and Nagarajaiah, S., *State of the art of structural control.* Journal of Structural Engineering, 2003. **129**(7): p. 845-856.
3. Rao, T.R.M., Rao, G.V., Rao, K.S., and Purushottam, A., *Analysis of passive and semi active controlled suspension system for ride comfort in an omnibus passing over a speed bump.* Analysis of Passive & Semi Active Controlled Suspension Systems, 2010. **5**: p. 7-17.
4. Yang, G., Spencer, B.F., Jr., Carlson, J.D., and Sain, M.K., *Large-scale MR fluid dampers: Modeling and dynamic performance considerations.* Engineering Structures, 2002. **24**(3): p. 309-323.
5. Bascom, W., *A hole in the bottom of the sea; the story of the mohole project*. 1961, Garden City, NY: Doubleday.
6. Lee, D.M. and Medland, I.C., *Base isolation-An historical development, and the influence of higher mode responses.* Bulletin of the New Zealand National Society for Earthquake Engineering, 1978. **11**(4): p. 219-233.
7. Sadek, F., Mohraz, B., Taylor, A.W., and M., C.R., *Passive energy dissipation devices for seismic applications*. 1996: National Institute of Standards and Technology, Building and Fire Research Laboratory.
8. Rana, R. and Soong, T., *Parametric study and simplified design of tuned mass dampers.* Engineering Structures, 1998. **20**(3): p. 193-204.

9. Friswell, M.I. and Inman, D.J., *The relationship between positive position feedback and output feedback controllers.* Smart Materials and Structures, 1999. **8**(3): p. 285.

10. Cheng, F.Y., Jiang, H., and Lou, K., *Smart structures: innovative systems for seismic response control*. 2010: CRC Press.

11. Soong, T., Reinhorn, A., Wang, Y., and Lin, R., *Full scale implementation of active control. I: Design and simulation.* Journal of Structural Engineering, 1991. **117**(11): p. 3516-3536.

12. Li, H. and Huo, L., *Advances in structural control in civil engineering in China.* Mathematical Problems in Engineering, 2010. **2010**.

13. Andrawes, B. and DesRoches, R., *Unseating prevention for multiple frame bridges using superelastic devices.* Smart Materials and Structures, 2005. **14**(3): p. S60.

14. Chiriac, H. and Stoian, G. *Influence of particle size distributions on magnetorheological fluid performances*. in *Journal of Physics: Conference Series*. 2010. IOP Publishing.

15. Gavin, H.P., *The effect of particle concentration inhomogeneities on the steady flow of electro-and magneto-rheological materials.* Journal of Non-Newtonian Fluid Mechanics, 1997. **71**(3): p. 165-182.

16. Rankin, P.J., Ginder, J.M., and Klingenberg, D.J., *Electro-and magneto-rheology.* Current Opinion in Colloid & Interface Science, 1998. **3**(4): p. 373-381.

17. Carlson, J.D. and Jolly, M.R., *MR fluid, foam and elastomer devices.* Mechatronics, 2000. **10**(4): p. 555-569.

18. Lokander, M. and Stenberg, B., *Improving the magnetorheological effect in isotropic magnetorheological rubber materials.* Polymer Testing, 2003. **22**(6): p. 677-680.

19. Zhou, G.Y., *Shear properties of a magnetorheological elastomer.* Smart Materials and Structures, 2003. **12**(1): p. 139.

20. Zhu, X., Jing, X., and Cheng, L., *Magnetorheological fluid dampers: A review on structure design and analysis.* Journal of Intelligent Material Systems and Structures, 2012. **23**(8): p. 839-873.

21. Carlson, J.D., *Low-cost MR fluid sponge devices.* Journal of Intelligent Material Systems and Structures, 1999. **10**(8): p. 589-594.

22. Liu, X.H., Fu, Z.M., Yao, X.Y., and Li, F., *Performance of magnetorheological fluids flowing through metal foams.* Measurement Science Review, 2011. **11**(5): p. 144-148.

23. Yan, Y.X., Hui, L.X., Yu, M., Fu, J., and Dong, L.H., *Dynamic response time of a metal foam magneto-rheological damper.* Smart Materials and Structures, 2013. **22**(2): p. 025026.

24. Li, W.H., Yao, G.Z., Chen, G., Yeo, S.H., and Yap, F.F., *Testing and steady state modeling of a linear MR damper under sinusoidal loading.* Smart Materials and Structures, 2000. **9**(1): p. 95.

25. Gavin, H.P., Hoagg, J., and Dobossy, M. *Optimal design of MR dampers*. in *Proceedings of US-Japan Workshop on Smart Structures for Improved Seismic Performance in Urban Regions*. 2001.

26. Nguyen, Q.H., Han, Y.M., Choi, S.B., and Wereley, N.M., *Geometry optimization of MR valves constrained in a specific volume using the finite element method.* Smart Materials and Structures, 2007. **16**(6): p. 2242.

Appendix A

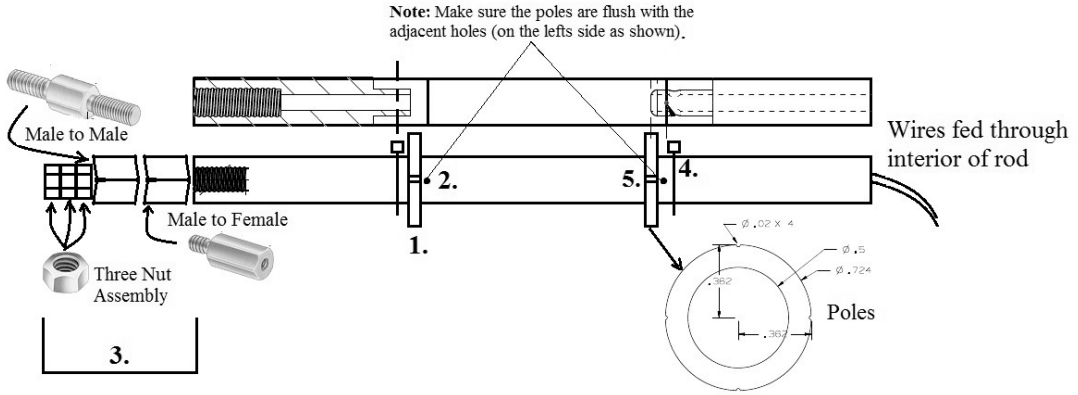

Figure A.1: Diagram for assembly of magnetic piston

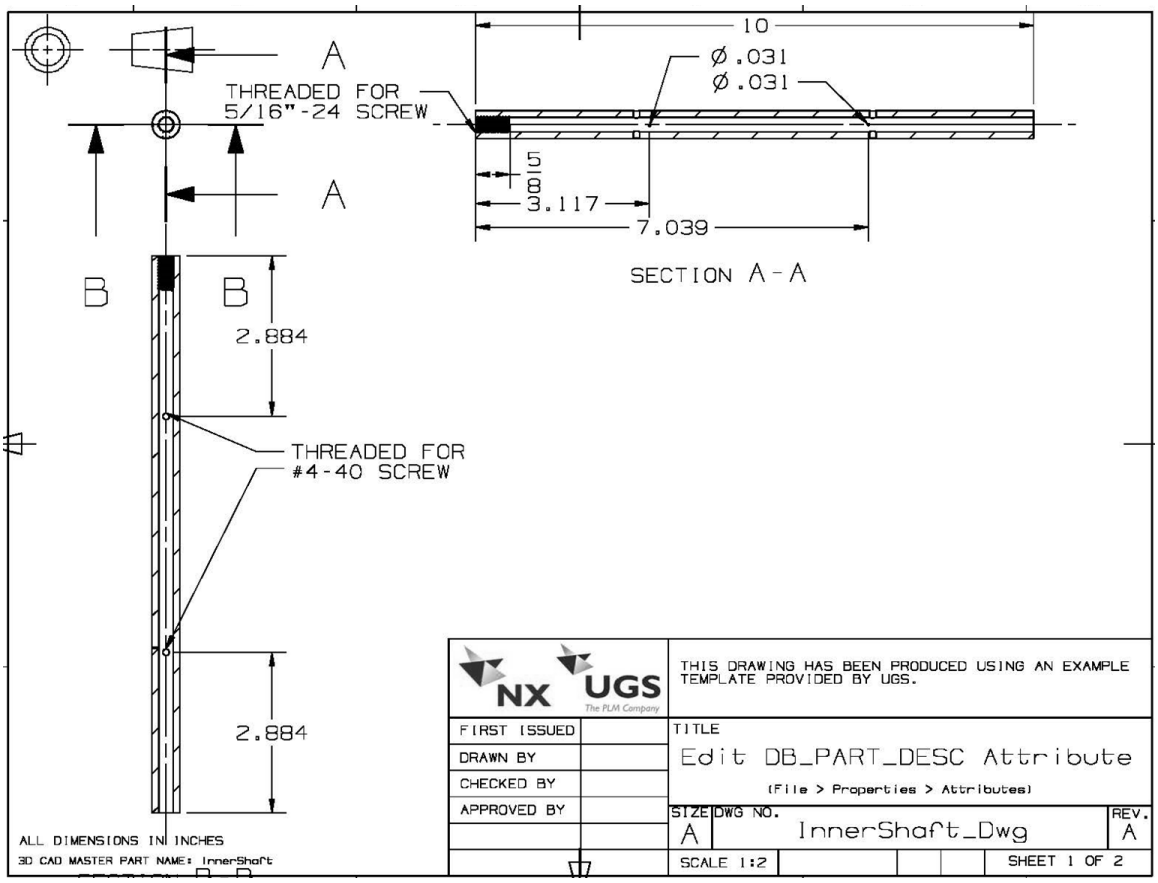

Figure A.2: Magnetic piston shaft dimensions

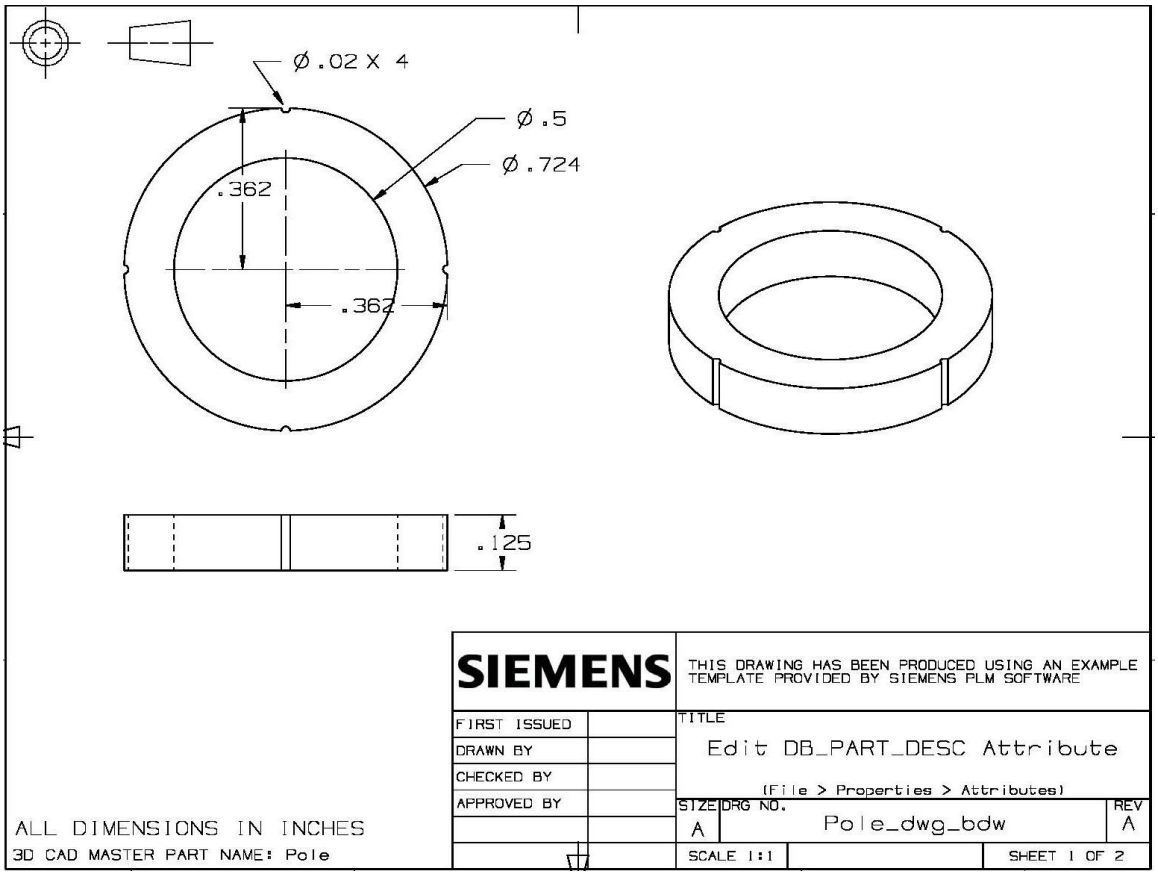

Figure A.3: Magnetic pole dimensions

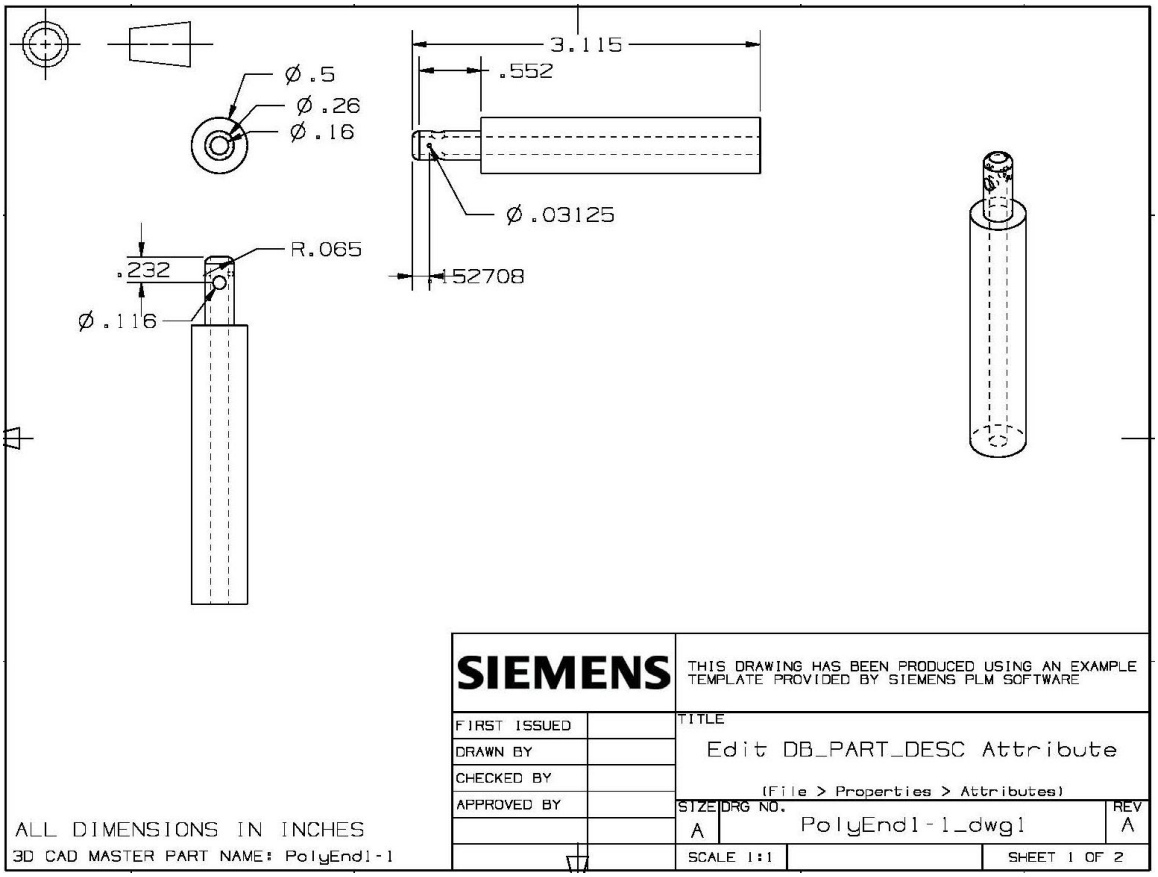

Figure A.4: Unthreaded Teflon piston shaft end

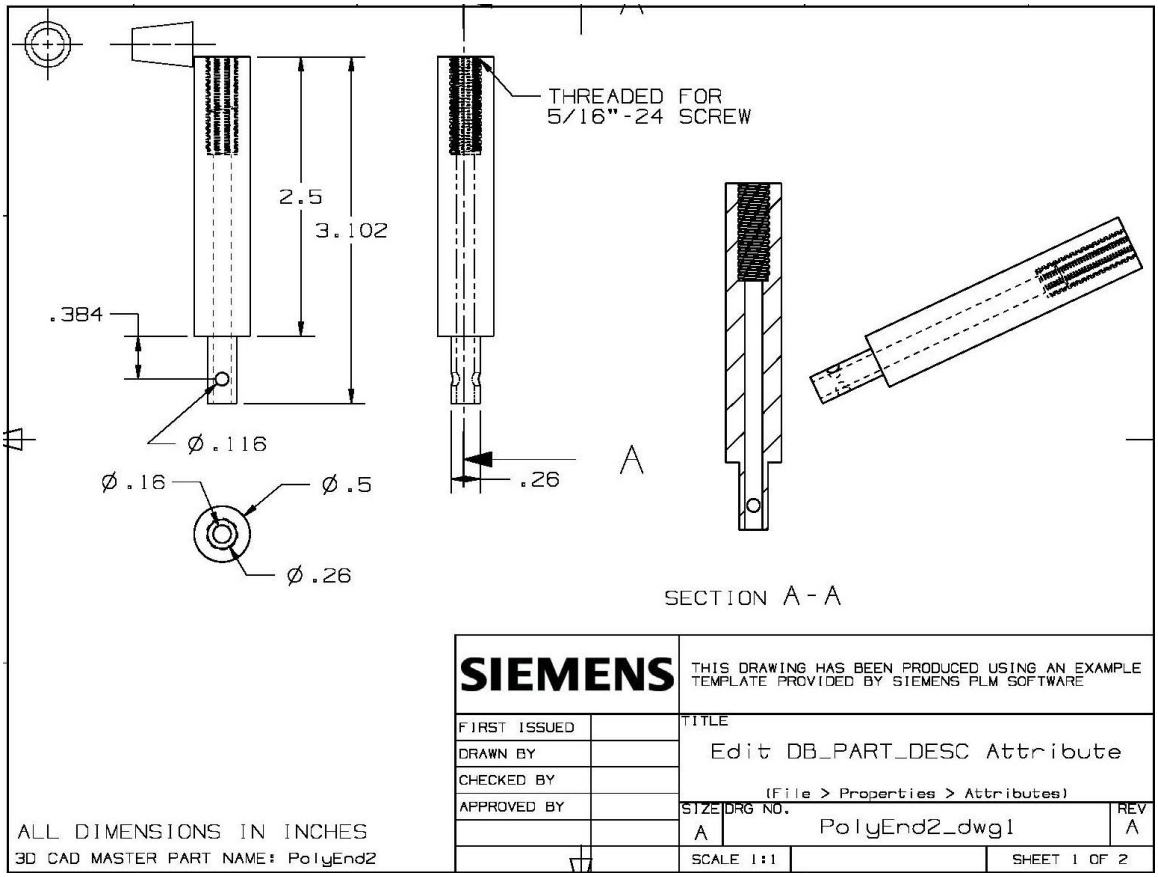

Figure A.5: Threaded Teflon piston shaft end

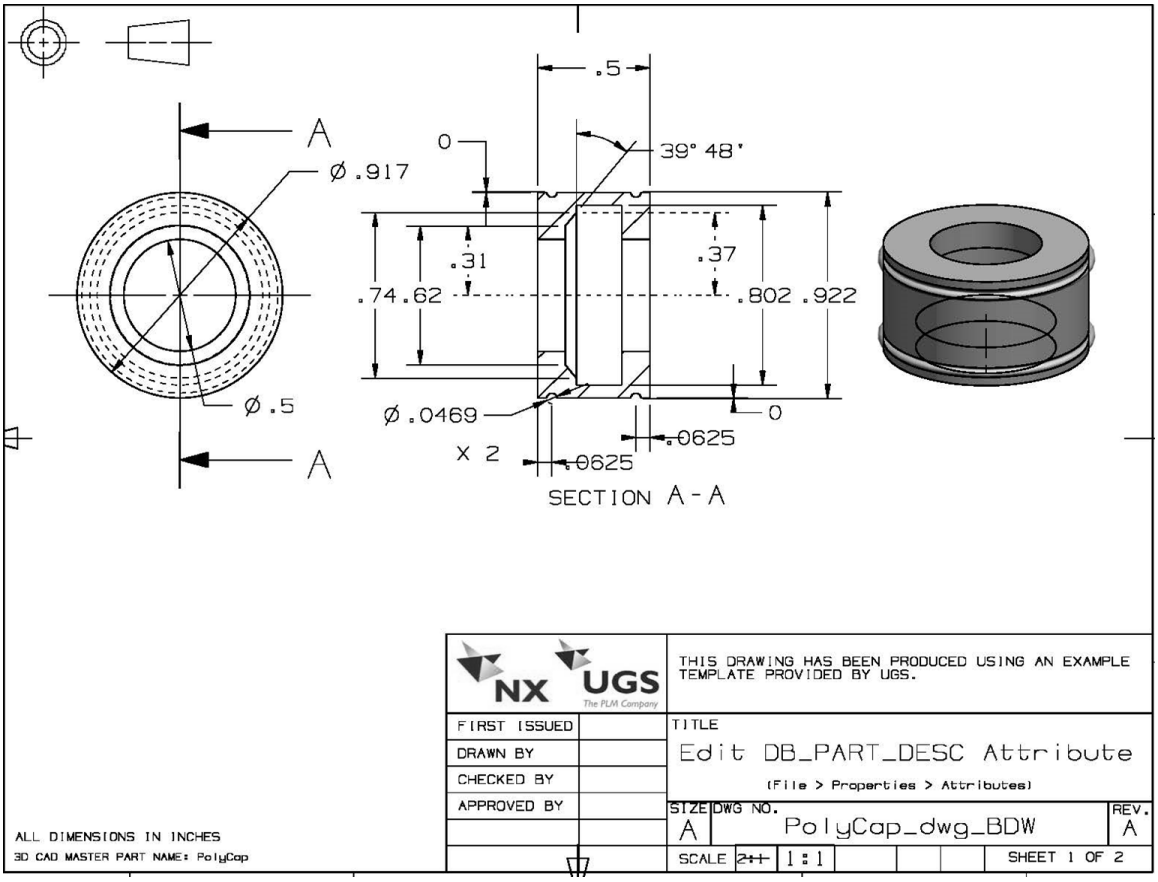

Figure A.6: Nylon cap for preliminary design

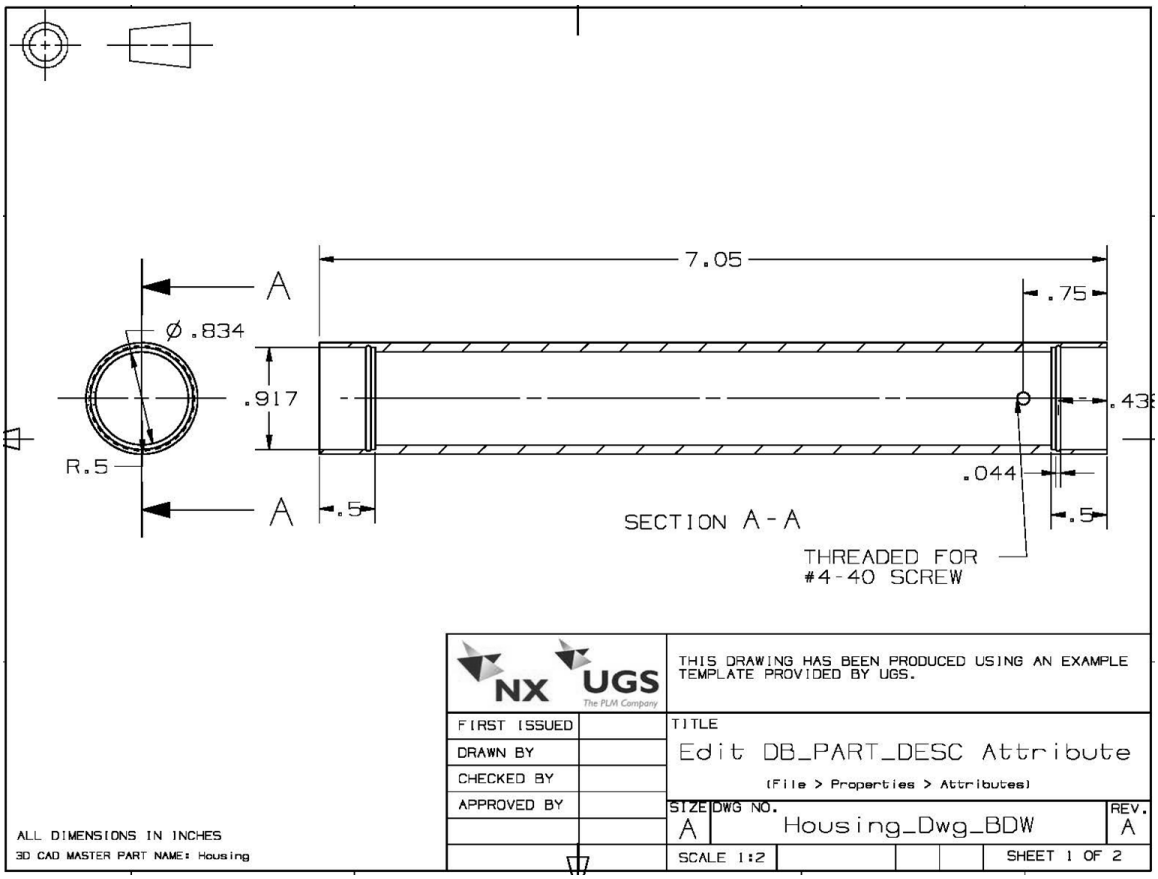

Figure A.7: Preliminary design housing dimensions

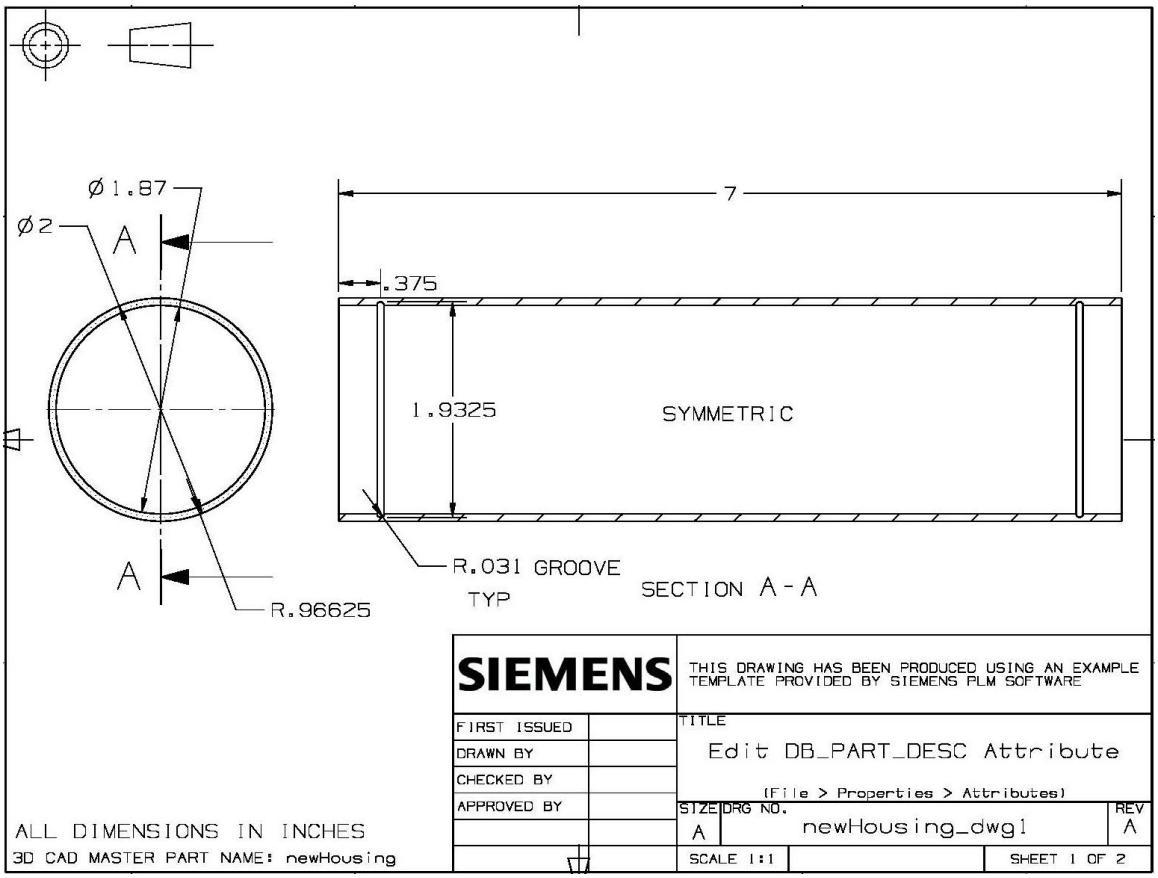

Figure A.8: Final design housing dimensions

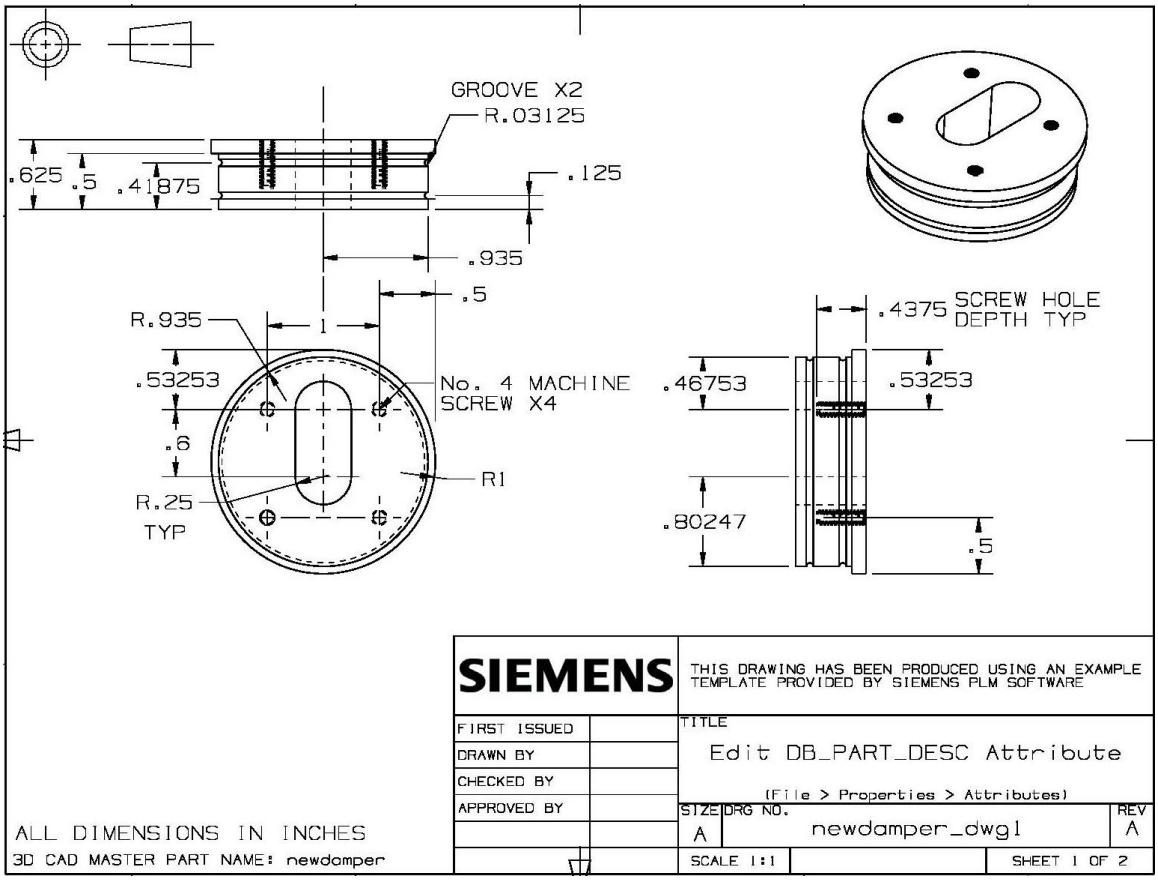

Figure A.9: Final design nylon piston guide dimensions